RESEARCH ARTICLE

Universal Grid-Forming Method for Future Power Systems

HANNU LAAKSONEN, (Member, IEEE)

School of Technology and Innovations, Flexible Energy Resources, University of Vaasa, 65200 Vaasa, Finland

e-mail: hannu.laaksonen@uwasa.fi

ABSTRACT Power system inertia typically refers to the energy stored in large rotating synchronous generators. Dynamics and stability of the traditional power system is closely linked to the natural inertia of these synchronous generators. In recent years, increasing amount of synchronous generators have been replaced by high amount of different type of inverter-based generating units connected at different voltage levels of the power system. Therefore, the dynamics and stability of future low-inertia power systems will be increasingly dominated by the control and synchronization of these inverter-based resources. One essential issue is that the typical grid-following control with phase-locked-loop (PLL) -based synchronization of inverter-based generation is not enough to guarantee frequency stability in future low-inertia power systems. Therefore, different grid-forming inverter control and synchronization methods have been proposed and developed. Currently there does not exist any universal grid-forming control and synchronization method. Therefore, this paper tries to propose a new universal frequency-locked-loop (U-FLL) -based synchronization method which is grid-forming for inverter-based generating units and grid-supporting for inverter-based loads. Advantageous operation of the new U-FLL synchronization and control strategy is confirmed by multiple simulations with different shares of inverter-based resources and synchronous generators in MV and HV hybrid power systems as well as with 100 % inverter-based LV, MV and HV networks.

INDEX TERMS Inverter-based resources, grid-forming, synchronization, frequency stability, low-inertia.

I. INTRODUCTION

The development of power systems in the direction of more flexible, resilient, digital and integrated energy systems needs a holistic multi-level systemic view and new enabling solutions. Future power system's increasingly sensitive dynamics and the adaptation capability to different variations, like inertia, renewables-based generation, fault levels and network topology, requires new flexibility service providers, compatible control and power system protection functions and enabling market schemes. Active (P) and reactive power (Q) control related flexibility services from different distributed energy resources (DER) will be needed for local (distribution system operator, DSO) and whole power system (transmission system operator, TSO) demand. Most common flexibility services are related to the control of the power system frequency (f) and local voltage (U) level. In general,

The associate editor coordinating the review of this manuscript and approving it for publication was Inam Nutkani.

flexibility services provision by DER can enable larger scale integration of renewable energy sources (RES) and electric vehicles (EVs) as well as minimize the whole system and societal costs. However, the effective utilization of flexibilities requires combination and coordination of different type and size of flexible energy resources from all voltage levels (LV, MV and HV). Therefore, flexibility services provision must be enabled by future-proof coordinated, adaptive and compatible DER control, management and protection schemes, regulation, market structures and business models. [1], [2], [3], [4]

Due to environmental reasons the traditional fossil fuel-based generation with large rotating synchronous generators (SGs) have been increasingly shutdown and the natural inertia of the power system has decreased. This is a risk for the power system frequency stability and requires new frequency control service providers as well as development of new future-proof frequency control related solutions. RES-based generation, like wind and PV, is connected to the power

system through power electronic inverter or power converter interfaces without natural inertia. Therefore, the frequency stability of future low, variable or zero inertia power system is greatly dominated by the control and synchronization methods of inverter-based resources (IBR). The dominant effect increases when the share of IBR-based generation in the power system is high compared to the SG-based generation. Stability in the future power systems with huge number of IBR-based resources at different voltage levels will be increasingly linked with the control schemes stability of IBRs. Therefore, understanding IBR-based generation control and synchronization methods will be crucial in the low or zero inertia power systems. [5], [6], [7], [8]

One major issue in realizing future low-inertia power system is that existing IBR-based generation control and synchronization is based on grid-following (GFL) control with PLL-component. GFL control assumes that power system frequency and voltage are controlled by traditional SGs with natural inertia. However, this GFL-based approach is not enough to guarantee frequency stability in future converter-dominated power systems with high share of IBRs. Therefore, grid-forming (GFM) control schemes, which can enable islanded microgrid operation, are also increasingly needed from IBRs during normal grid-connected operation. More importantly, future resilient hybrid power systems with variable share of GFM- and GFL-controlled IBRs and SGs must remain stable in all situations and also be capable of operating in several islands (microgrids) if needed. In order to achieve this new universal, stable and stability supporting grid-forming IBR-control schemes are needed. [9], [10]

In this paper, new universal grid-forming and supporting frequency-locked-loop U-FLL-based control and grid synchronization for IBRs is proposed (Section III). In overall, the target of the U-FLL is to be applicable different type of future low-inertia power systems with different share of rotating SGs and IBRs. The proposed U-FLL scheme and its other general targets are described with more details in Section III.

In the following, Section II provides a state of the art review regarding control and grid synchronization methods for IBRs. Section III presents the proposed new grid-forming/-supporting U-FLL synchronization method for IBRs. Then, Section IV presents the study cases and simulation models with different shares of IBRs and SGs in MV and HV hybrid power systems as well as with 100 % IBR-based LV, MV and HV networks. Thereafter, the simulation results are presented in Section V to confirm the operation of the new U-FLL-based synchronization method. Finally, conclusions are stated in Section VI.

II. IBR CONTROL AND GRID SYNCHRONIZATION -STATE -OF -THE ART
A. TYPICAL IBR CONTROL AND SYNCRONIZATION METHODS
In the following, typical IBR control and synchronization methods for GFL and GFM inverters are reviewed based on the literature. GFL inverter is typically described and approximated as a controlled current source with high parallel impedance and GFM inverter as a voltage source with low series impedance [11], [12]. There is no official formulation and definition for GFM control [11]. However, it is under discussion [13], [14] and e.g. in [15] a proposal for the definition of GFM capability and synchronization services have been made in the following manner: "A GFM unit shall be capable of self-synchronization, standalone and provision of synchronization services, which means that it does not rely on grid conditions to synchronize and will help other units to maintain synchronism, while still complying with other general requirements applying to the specific technology.".

Synchronization processes of GFL and GFM inverters are one of the main differences between them. In overall, many grid synchronization schemes [16], [17], [18], [19] have been previously proposed for inverter-based DER with a focus on immunity to disturbances (e.g. harmonics, voltage fluctuations, faults) and synchronization stability in weak grids [6]. Typically a GFL inverter utilizes voltage-based grid synchronization [6] which means that GFL unit is synchronized to measured or estimated grid voltage angle e.g. by PLL or frequency-locked-loop (FLL) component. On the other hand, many of the GFM inverter control methods do not need a PLL or FLL and GFM control schemes can be based e.g. on power synchronization [6], [20] to emulate the power synchronization principles of SGs [11]. One main difference between GFL and GFM behavior can be also seen in their response to a network disturbance (like fault), and their small-signal operation when connected to a weak or stiff grid [11] (see Section II.B). Table 1 presents a basic overview about main features and differences related to GFL and GFM inverter control and synchronization principles (mainly based on [10]).

Previously, multiple alternative GFM control schemes have been proposed and presented in [6], [11], and [21], like

1) Droop-Based Grid-Forming Control Methods (e.g. the basic control and control using low-pass filter),
2) Power Synchronization Loop / Power Synchronization Control (PSC)
3) Voltage Controlled Inverter (VCI)
4) Virtual Synchronous Machine (VSM) / Virtual Synchronous Generator (VSG)
5) Virtual Oscillator Control (VOC) / dispatchable Virtual Oscillator Control (dVOC)
6) Matching Control
7) PLL-Based Modified Current-Control Methods and
8) Direct Power Control (DPC).

Droop-based grid-forming control methods and power synchronization control are the most common GFM control schemes and can be also seen equivalent to each other [6]. On the other hand, for example, VOC-based GFM control scheme is quite recent nonlinear method which allows converters to synchronize with each other without any communication between them [11]. In addition, different modified

GFL inverter	GFM inverter
Approximated as a controlled current source with high parallel impedance	Approximated as a voltage source with low series impedance
Expects grid is already formed	Expects it will form and maintain the grid
Typically needs PLL or FLL for voltage-based grid synchronization	Typically does not need PLL or FLL and utilizes power-based synchronization (However, PLL-based GFM control is also possible [21]-[23])
DQ-based current control	Voltage magnitude and frequency/phase control
Decoupled control of P and Q (+)	Slight coupling between P and Q control (-)
Cannot be used for black-start i.e. needs voltage at the connection point to be able to inject P and Q (-)	Can be used for black-start of a power system (e.g. microgrid) (+)
Cannot operate at 100 % IBR-based grids without any GFM-controlled IBRs and SGs (-)	Can theoretically operate at 100 % IBR-based grids (like microgrids) without SGs and together with GFL-controlled IBRs (+) (However, there is not much practical experience at the moment about larger power systems)

+ Positive feature, - Negative feature

VSM/VSG control schemes have also been proposed quite recently e.g. in [24], [25], [72], and [73]. Advantages and disadvantages of different current and voltage-based VSG control schemes have been summarized and compared in [75].

B. ISSUES WITH IBR CONTROL AND SYNCHRONIZATION

Previously, GFM control schemes have been utilized in different microgrid and uninterruptable power supply (UPS) solutions. However, there is not much experience from larger power systems in which large amount of GFM IBRs should replace large traditional rotating SGs. In addition, there are no universal or standardized GFM control scheme at the moment (see Section II.A). Therefore, there are some serious concerns about frequency stability and control related to fully or mainly IBR-based larger power systems [26]. For example, [27] presents a system operator research agenda for future power systems and one of the six main research themes is related to inverter design.

Regarding GFL-based inverters' control stability, it has been stated in [11] that studies about negative small-signal stability effects of GFL inverters' PLLs [28], [29], [30] have shown that also the interactions (i.e. induced sideband oscillations around nominal frequency [6]) between PLLs of different nearby GFLs become stronger when the short-circuit ratio (SCR) of grid is reduced (i.e. in weak grids). On the other hand, it has been presented in [31] and [32] that GFM inverters are suitable for weak grid applications. However, GFMs are more susceptible to instability in stiff

grids [11], [33], [34] and series compensated grids [6], [35] when compared to GFLs. In stiff grids small change of the phase difference between the GFM inverter and grid voltages can lead to large active power variations [5], [11], [33].

In [26], the large-scale deployment GFMs and their effect on frequency behavior was studied. The presented results suggested that, with sufficient controller tuning, frequency stability could be maintained. However, the changed power system dynamics (for example, steady state can be reached much faster in 100 % IBR-based system) may require settings adaptation in protection and load shedding functions due to changed frequency nadir and rate-of-change-of-frequency (ROCOF). In addition, there is a need for power system stabilizers (PSSs) which can handle a variable amount of IBR-based generation. In [11] some issues and challenges regarding GFM inverters, like angle stability, fault ride-through (FRT) capability, and transition from islanded to grid-connected mode have also been presented and discussed. [36] emphasized that the unintentional islanding of GFM inverters can be also a new risk to the reliability of future IBR-based power systems, because the variables that are used for islanding detection of GFMs are different than with GFLs.

Previously, methods that combine traditional GFL and GFM inverter synchronization methods, like PLL and power-synchronization, have also been proposed in [37], [38], and [39]. In these schemes, the power-synchronization has been the main synchronization method and the PLL was used to extract the grid frequency as input for the internal damping controller [40]. During large disturbances like significant grid faults or loss of a large generation/load, the small-signal analysis is not sufficient to describe the synchronization dynamics of IBRs [6]. Therefore, distorted, faulty and unbalanced grid voltages are challenging for all synchronization methods [40]. To overcome these challenges, improvements for both PLL- [17], [41] and power-based synchronization [20], [42], [43] methods in faulty grids have been proposed [40]. It has been stated that the PLL introduces a second-order nonlinear swing equation to GFL inverters and, instead of traditional power-angle curve, a voltage-angle curve [6], [44]. On the other hand, droop-controlled GFM inverters can be characterized as a first-order nonlinear system, which improves the transient stability [6], [45]. However, reactive power droop control loop can negatively affect the transient stability of GFMs [6], [46]. Unlike with SGs, the limited overcurrent capability of IBRs requires the use of current limiting control [6], which places another constraint to the transient stability of GFMs [6], [47]. Table 2 presents, in addition to Table 1, summary about advantages and disadvantages of GFL and GFM inverters (mainly based on [59] and references in this Section II.B). However, it can be emphasized that each GFM control scheme do not have all the advantages and disadvantages mentioned in Table 2.

In overall, the role of inverter-based generation stability issues will be substantial in future power systems and requires also new stability definitions [48]. In [49] the potential forthcoming power system stability issues with increased

TABLE 2. Summary about advantages and disadvantages of GFL and GFM inverters (modified from [59], see also Table 1).

	GFL inverter	GFM inverter
Advantages (+)	• Simple controls • Very fast response time • Suitable for DC bus voltage control • Suitable for RES grid interface • Available in rotating and stationary frames • Automatically limits current during faults	• Grid master • Can run in stand-alone (microgrid) mode • Can run in weak grids • Handles load changes without disturbance • Droop-controlled GFM inverters can improve the transient stability (see also possible disadvantages)
Disadvantages (-)	o Does not contribute to grid strength (support grid) o Requires a stiff grid (In weak grids a) interactions between PLLs of different nearby GFLs become stronger, b) complexity and hierarchy of control layers and the coordination and interoperability of these fast controls may be a challenge) o PLL loses track of grid frequency during faults o Cannot be grid master o Limit to percentage on a grid o PLL introduces a second-order nonlinear swing equation to GFL inverters and also a voltage-angle curve o Unstable low-frequency oscillations with GFLs can exist due to different forms of interaction between the controllers of the IBRs and other system components	o Desynchronizes during faults o Too stiff in pure form (Sensitive to instability in stiff grids and series compensated grids) o Does not share with legacy SGs o May require adaptation of protection and load shedding settings o Transition from islanded to grid-connected mode is a challenge o Unintentional islanding of GFM inverters can be a risk o Reactive power droop control loop can negatively affect the transient stability of GFMs o Current limiting control places constraint to the transient stability of GFMs o Coupling between active (P) and reactive power (Q) negatively affects the dynamic performance and stability of GFMs o Destabilizing interaction between the fast synchronization of GFMs and the slow response of other SGs is possible

amount of IBR-based generation are presented and also the differences between traditional SGs and IBRs from dynamic behavior (e.g. after fault clearance) viewpoint are shown. Also learnings from different sizes of power systems are described in [49]. It has also been stated in [48] and [49] that when IBR penetration increases, also the complexity and hierarchy of control layers grows and the coordination and interoperability of these fast controls (outer power and voltage control loops and PLL) with GFLs to maintain stability is becoming increasingly difficult, especially in weak grids [50]. In [48] it has also been reported that unstable low-frequency oscillations in power systems with GFLs can exist due to different forms of interaction between the controllers of the IBRs and other system components. Harmonic

stability [18] is also one potential challenge of IBR-based future power systems. [51] also highlights that the coupling between active (P) and reactive power (Q) negatively affects the dynamic performance and stability of GFMs.

Small- and large-signal stability studies and analysis [52], [53], [54], [55], [56], [57] are important in order to develop future-proof control and synchronization solutions for future hybrid power systems with different about of GFMs, GFLs and SGs. Also, for example, in [58] the impact of the GFMs on the frequency stability of SGs was studied and it was concluded that after loss of a SG destabilizing interaction between the fast synchronization of GFMs and the slow response of other SGs is possible.

C. PROPOSED IBR CONTROL AND SYNCHRONIZATION SCHEMES

In the literature multiple modified and improved control strategies have been proposed in order to solve different control and synchronization challenges (Table 2) of IBRs. For example, in [6] different stabilizing methods (to improve small-signal and transient stability) for GFLs and GFMs as well as current limiting schemes for GFMs are presented based on multiple references which are also summarized in six separate tables. In addition, [40] provides good overview about potential model and data-based advanced control methods. Also, for instance, in [60] a generalized multi-input-multi-output-based GFM (MIMO-GFM) control architecture combining multiple different GFM control schemes (Section II.A) has been proposed in order to improve GFM units' performance.

New GFL inverter control schemes have also been proposed, for example, in [61], [62], [63], [64], and [65] to enhance the PLL-based grid synchronization stability of GFLs in weak grids. In addition, for example, [66] proposed an universal controller to enable different combinations of two GFM (PSC) and GFL (vector current control (VCC)) schemes to be studied so that PSC is used as a guideline for a robust VCC design, permitting stable control in both weak and stiff grids. In order to improve traditional PLL-based GFL inverter grid synchronization under voltage unbalance and harmonic distortion different FLL-based synchronization schemes, e.g. [67], and its improvements have been proposed in [68], [69], [70], and [71].

III. NEW UNIVERSAL GRID-FORMING METHOD
A. GENERAL TARGETS
Although lot of research has been done on GFMs, no universal grid-forming control and synchronization method currently exists and many previously proposed methods have different drawbacks and challenges (see Section II). Some of the previously proposed GFM control methods have steady-state frequency deviation during 100 % IBR-based systems (e.g. microgrids). Therefore, this paper proposes new universal grid-forming/-supporting U-FLL-based synchronization

for IBRs. General targets for the new U-FLL were the following:

1) Applicability on to different type of variable inertia, hybrid power systems (from high to low or zero inertia i.e. without SGs) and utilization capability for intended islanded microgrid operation (supporting resilient and flexible future power systems)
    - Different share of SGs and GFM-/GFL-based generation
    - Weak and stiff grids as well as MV and LV microgrids
2) Possibility to retrofit the existing PLL-based GFL control schemes with grid-forming/-supporting U-FLL component
3) Consider also the possibility of making or even retrofitting PLL-based grid-following inverter-based loads with U-FLL component to be grid-supporting (in terms of frequency and synchronization stability, including e.g. EV/BESS charging, hydrogen electrolyzers etc.)
4) Zero steady-state frequency deviation during 100 % IBR-based operation (e.g. islanded microgrid operation) from nominal frequency unlike typical droop-based GFM control schemes
5) Compatibility of U-FLL with current grid code requirements (e.g. fault behavior and fault-ride-through), system-level (TSO) market structures (e.g. related to frequency control with active power-frequency (Pf) -droop), local (DSO) and system-level (TSO) voltage control methods (e.g. reactive power-voltage (QU) -droop) as well as protection and islanding detection schemes
    - Target of U-FLL method is not to try to act as VSM/VSG
    - Unlike in many droop-based GFM and self-synchronized droop or VSG control schemes, in the proposed U-FLL method active and reactive power control loops are decoupled from synchronization method on purpose
    - Target is to enable universal compatibility in provision of different P and Q related flexibility services under different grid and market conditions & requirements including real-time adaptive Pf-, QU- and PU-droops in order to maximize flexibility services value locally for DSOs and system-wide for TSO
6) Compatibility with existing passive islanding detection schemes.

B. DEVELOPMENT BACKGROUND

In order to achieve the above mentioned targets (see Section III.A), the possibilities to create universal grid-forming and supporting PLL by modifying traditional synchronous dq-frame grid-following PLL (Fig. 1a) [74] were first evaluated. To improve the performance of synchronous
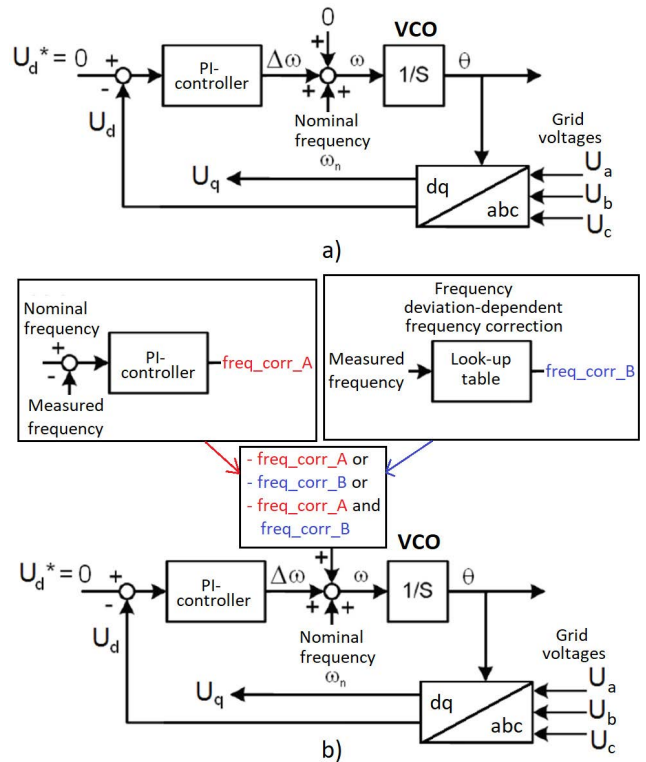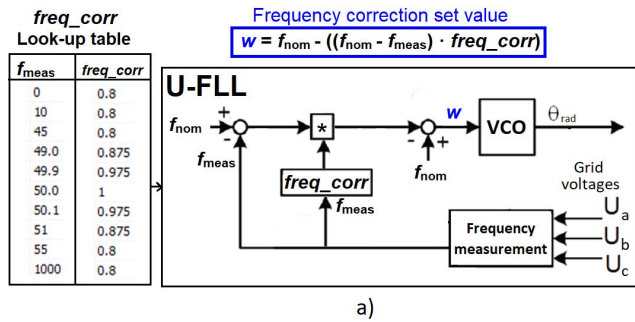

FIGURE 1. a) Grid synchronization method with synchronous *dq*-frame grid-following PLL [74] and b) Evaluated modified grid-forming and supporting synchronous *dq*-frame PLL schemes.

dq-frame PLL (Fig. 1a) during unbalanced conditions and disturbances, input phase voltages were negative sequence filtered in all cases. Fig. 1b) presents the evaluated modified grid-forming and supporting synchronous dq-frame PLL schemes.

However, it was realized during the development work and simulation studies that achievement of targets (Section III.A) and universal synchronization method is very difficult, also partly due to general stability related challenges of PLLs with PI-controllers as described in Section II.B and Table 2 regarding GFLs. Therefore, during further development work one target was also to minimize or remove the challenges related to the PLLs' fast PI-control loops with GFL-based IBRs. In addition, it was found out that in hybrid power systems with IBRs and SGs, the voltage phase angle of grid-forming IBR should be close enough to SG's phase/rotor angle during frequency and phase angle oscillations after disturbances (e.g. load, generation or topology changes, like e.g. red curve in Fig. 3) in order to maintain synchronism and support the transient frequency and synchronization stability of the power system. Achievement of this was also very challenging with modified PLL-based schemes (Fig. 1b) and better methods were needed. On the other hand, GFM synchronization schemes with fixed nominal frequency input (see Fig. 4), which could be used in islanded microgrids with one master unit, are not universally applicable and not able to fulfill targets described in Section III.A.

a)

b)

FIGURE 2. a) Proposed universal grid-forming and supporting U-FLL synchronization method and b) PSCAD implementation of U-FLL.

FIGURE 3. The difference between the measured frequency (f_{meas}) and the frequency correction set value (w) (see also Fig. 2 and Eq. (1)).

C. PROPOSED NEW METHOD

In the descriptive name of the proposed new U-FLL method, the role of using measured grid frequency as the main input parameter was chosen to be emphasized instead of voltage phase like in PLL. Fig. 2 presents the PSCAD implementation of the proposed new universal grid-forming/-supporting U-FLL synchronization method which does not include any PI-controller like PLL-based method presented in Section III.B (Fig. 1). In the proposed new U-FLL method, the frequency correction set value w of U-FLL (see Fig. 2 and Eq. (1)) was introduced. The value of w is input to voltage-controlled oscillator (VCO) and it should be smaller (i.e. closer to nominal frequency) than the measured frequency f_{meas} (see Fig. 3). In Eq. (1) *freq_corr* parameter is

a frequency correction coefficient i.e. adaptive (frequency-dependent) coefficient in Fig. 2.

$$w = f_{nom} - ((f_{nom} - f_{meas}) \cdot freq\_corr) \qquad (1)$$

In the PSCAD implementation of U-FLL (Fig. 2b) measured frequency f_{meas} from FFT-component was utilized. However, also other stable measured frequency inputs can be used with U-FLL. In this paper nominal frequency f_{nom} is 50 Hz. As shown in Fig. 2, it was also determined that the *freq_corr* -coefficient could be adaptive and measured frequency f_{meas} dependent. This means that during larger frequency deviation, the *freq_corr* -coefficient would be smaller in order to provide more frequency and synchronization stability support. The basic idea behind this can be seen from Fig. 3 where blue line presents the measured frequency (f_{meas}) and red line the frequency correction set value (w).

Small and large-signal stability of the GFM and GFL synchronization methods during steady-state operation and disturbances is vital for the stability of the future power system. In order to guarantee the stability of U-FLL in different type and size of power systems as well as with different type of DER units and control schemes, multiple study cases were chosen to be included in Section IV of this paper. In this paper, focus is on the frequency stability improving grid-forming and supporting performance of U-FLL after transition from grid-connected to islanded operation as well as after connection of large load. In order to focus purely on the effect of grid-forming and supporting U-FLL on frequency stability, *Pf*-control of U-FLL based DER unit is not included in the studies of this paper. Therefore, U-FLL stability during severe faults, U-FLL based DER unit's compatibility with active and reactive power control related technical ancillary / flexibility services, like *Pf*-, *QU*-, *PU*-control and corresponding grid codes and market schemes as well as compatibility with traditional passive islanding detection schemes will be reported in further studies.

During the development of the proposed new U-FLL also the effect of *freq_corr* -value on the stability of U-FLL and corresponding DER unit control scheme has been studied in different cases. Based on those studies the values used in the *freq_corr* -look-up table (Fig. 2a) were chosen. In general, U-FLL and other GFM schemes should be also stable during extreme cases, like long duration frequency deviations in power systems having limited share of U-FLL based generation. The challenge can be, that the stability of DER unit control is lost if the U-FLL output phase angle θ_{rad} (Fig. 2a) deviates too much and/or too long (e.g. constant over $\pm$ 0.5 Hz over- or under-frequency for a few minutes) from the real voltage phase angle (e.g. followed by traditional PLL). Therefore in order to prevent this kind of potential instability of U-FLL, for example, cumulative phase angle difference monitoring logic needs to be included in U-FLL. This logic can ensure stability, grid-forming operation and frequency FRT capability of the DER unit, but momentarily reduces the frequency stability supporting effect of U-FLL.
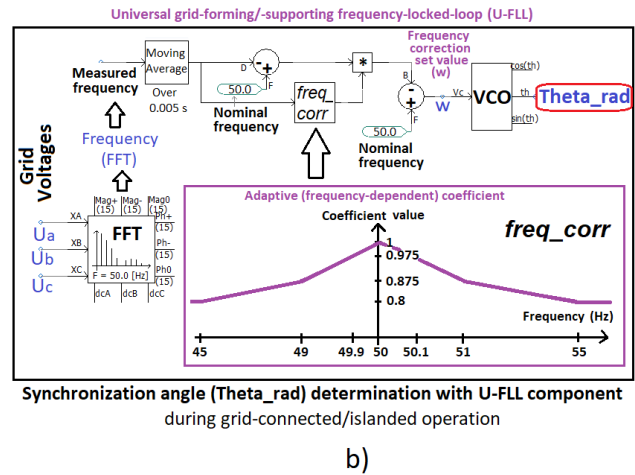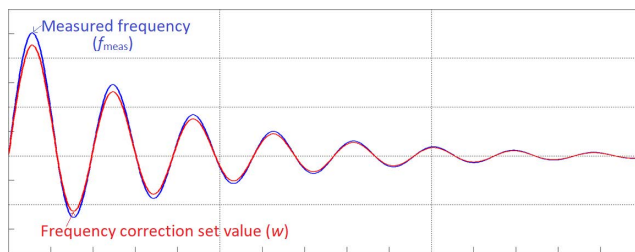
IV. STUDY CASES AND SIMULATION MODELS

Many inverter control focused studies are done with very simplified power system models (e.g. in terms of lines, transformers, loads) and amount of inverters (e.g. single inverter) which in some cases may lead to inaccurate conclusions about the performance of the proposed control scheme and does not reveal, for example, potential mutual effects between different IBRs (with different GFL and GFM control schemes), between grid components as well as neglects the role and effect of different IBRs location in the power system.

In order to study and confirm the operation and applicability of the proposed new grid-forming/-supporting U-FLL in a versatile manner and to avoid possible inaccurate conclusions based on studies with very simple models, multiple PSCAD simulation studies were done with different share of IBR-based generation. The main study cases of this paper are summarized in Table 3.

TABLE 3. Main study cases.

Case	Voltage level	Type and number of generating units	Synchronization of IBRs
CASE_1_MV_HYBRID	MV	WT (1, full power conv.), SG (1)	PLL or U-FLL
CASE_2_HV_HYBRID	HV	BESS (16/28), SG (1)	PLL or U-FLL
CASE_1_MV_IBR / CASE_1_LV_IBR	MV and LV	WT (1, full power converter), BESS (1)	U-FLL
CASE_2_HV_IBR	HV	BESS (68)	U-FLL

The main simulation cases (Table 3) included:

a) Different type of DER units with traditional PLL-component for grid synchronization (PLL was replaced by the new U-FLL -component, Fig. 2)
   ○ Wind turbine (WT) with full power converter, detailed model including power electronic switches, connected in MV network (Fig. 4)
   ○ Battery energy storage system, BESS with AC/DC-inverter, detailed model including power electronic switches, connected in LV network, operation in discharge mode (generation) (Fig. 5)
   ○ BESS, average model controlled voltage sources, without power electronic switches in order to reduce the needed simulation time, connected in MV network, operation in discharge and charge modes (generation and load) (Fig. 6)

b) Different DER unit combinations in various type and size of power systems and at different voltage levels
   ○ Hybrid with IBR and synchronous generation (SG)
   - WT (MV network, Fig. 4) and SG (MV network), grid-connected and MV islanded operation, (CASE_1_MV_HYBRID) (Fig. 7)
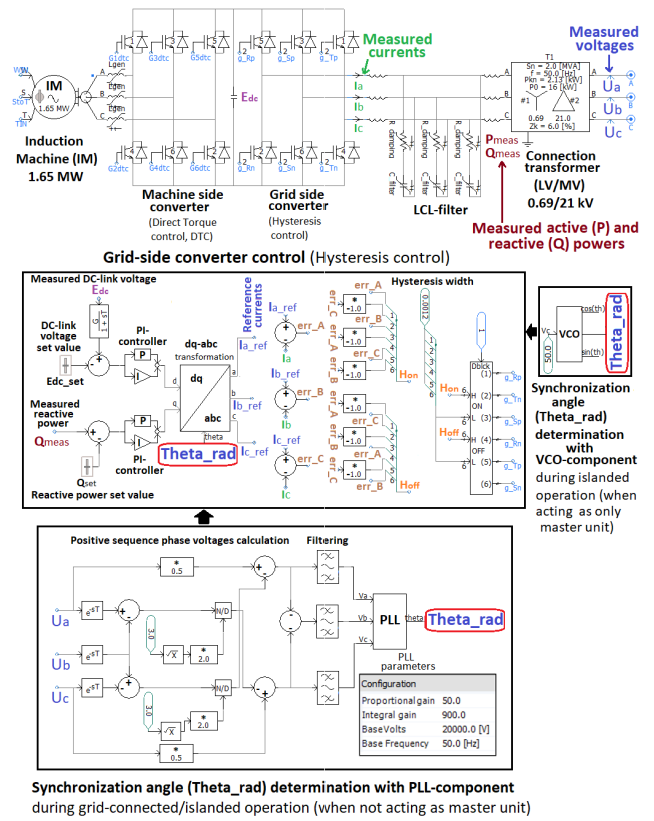   - 16 BESSs (MV network, Fig. 6) and SG (HV network, Fig. 8), small HV network

FIGURE 4. Detailed PSCAD model of wind turbine, WT, with full power converter control scheme without utilization of new U-FLL (Fig. 2) in CASE_1_MV_HYBRID (Fig. 7) and CASE_1_MV_IBR (Fig. 10).

islanded operation, BESSs both in discharging (CASE_2A_HV_HYBRID) and charging (CASE_2B_HV_HYBRID) operation (Fig. 9)
   ○ 100 % inverter-based resources (IBR)
   - WT (MV network, Fig. 4) and BESS (LV network, Fig. 5), grid-connected and MV islanded operation, (CASE_1_MV_IBR) (Fig. 10)
   - BESS (LV network, Fig. 5), LV islanded operation, (CASE_1_LV_IBR) (Fig. 10)
   - 68 BESSs (MV network, Fig. 6) small HV network islanded operation, discharging operation, (CASE_2_HV_IBR) (Fig. 11)
   c) For example, following issues were studied and compared in the study cases (see Table 3 and Section V)
   ○ Hybrid (MV), CASE_1_MV_HYBRID, (Fig. 7)
   - Base cases with traditional PLL and grid-following / grid-forming control of SG
   - Frequency and synchronization stability after transition to MV islanded (microgrid) operation, effect of U-FLL, focus on first swing of SG
   - Effect of different U-FLL freq_corr -coefficients
   ○ 100 % IBR (MV & LV), CASE_1_MV_IBR and CASE_1_LV_IBR (Fig. 10)
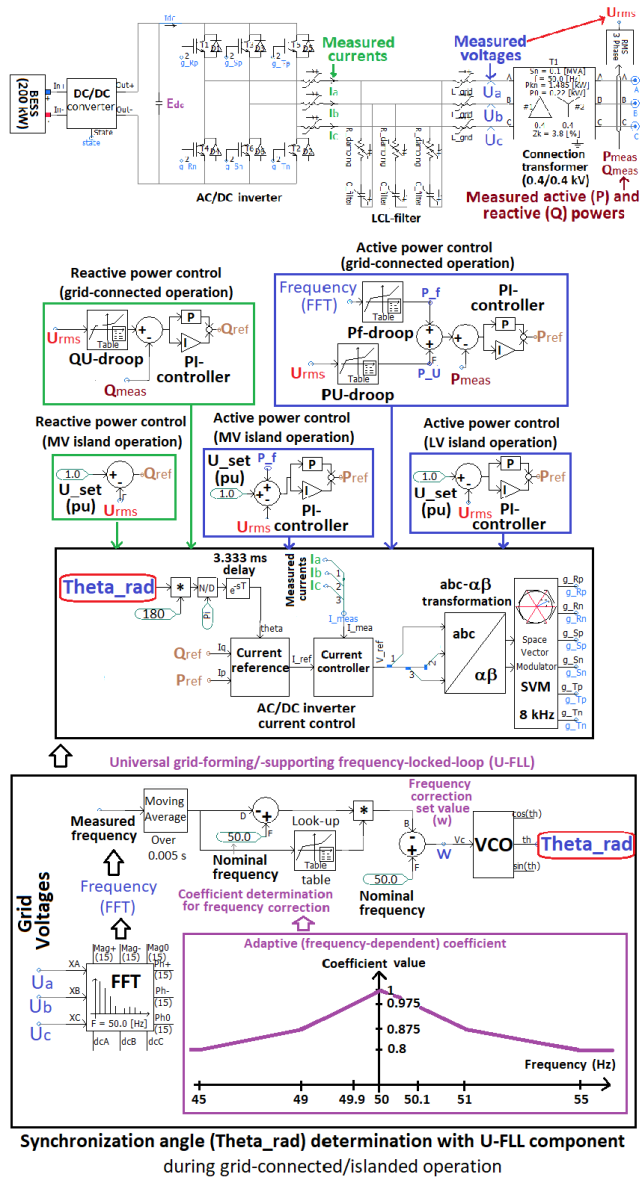   - Effect of different U-FLL freq_corr -coefficients

FIGURE 5. Detailed PSCAD model of battery energy storage system, BESS with AC/DC-inverter control scheme including new U-FLL (Fig. 2).

- Frequency and synchronization stability after transition to MV or LV islanded (microgrid) operation, effect of U-FLL
  ○ 100 % IBR (HV), *CASE_2_HV_IBR* (Fig. 11)
- Frequency and synchronization stability after load change with only U-FLL-based DER
  ○ Hybrid (HV), *CASE_2A_HV_HYBRID* and *CASE_2B_HV_HYBRID* (Fig. 9)
- BESSs both in discharging (*CASE_2A_HV _HYBRID*) and charging (*CASE_2B_HV _HYBRID*) operation
- Frequency and synchronization stability after load change, effect of U-FLL, focus on first swing of SG
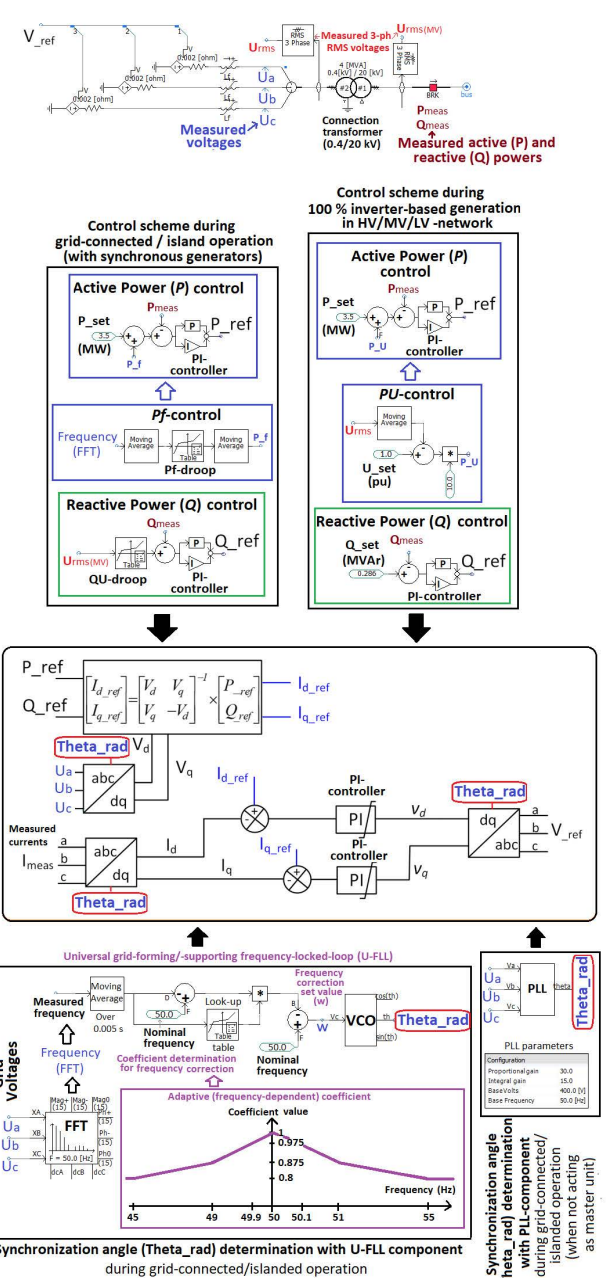
FIGURE 6. BESS's average PSCAD model with controlled voltage sources and control scheme with new U-FLL (Fig. 2) or traditional PLL.

V. SIMULATION RESULTS

In the following, the main simulation results from different study cases (see Section IV) are presented. First, in Section V.A results from hybrid MV microgrid (*CASE_1_MV_HYBRID*, Fig. 7 and Table 3) simulations are presented. Then, Section V.B shows the results from cases with 100 % IBR-based generation in MV and LV microgrids (*CASE_1_MV_IBR* and *CASE_1_LV_IBR*, Fig. 10 and Table 3). Next, in Section V.C the simulation results from case with 100 % IBR-based generation in small HV network (*CASE_2_HV_IBR,* Fig. 6 and Table 3) are presented.
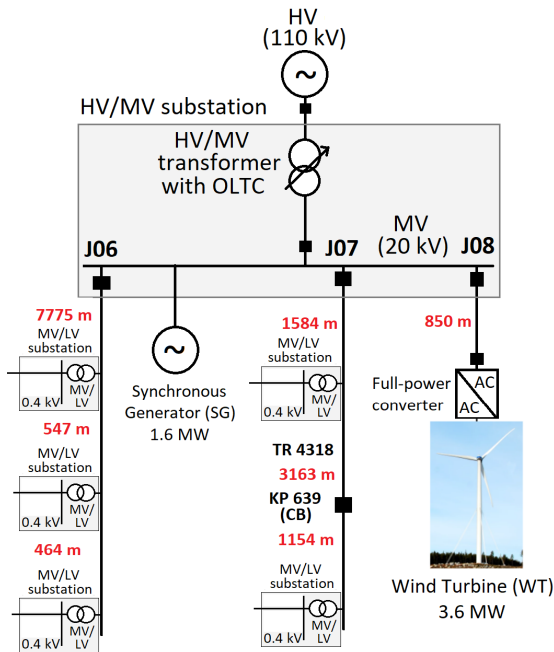
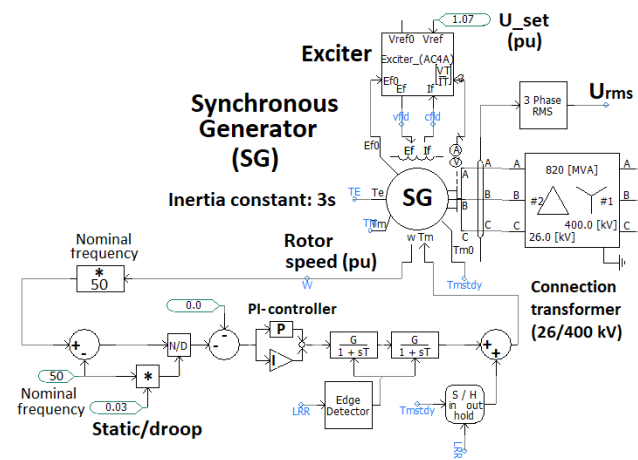**FIGURE 7.** One-line diagram of the MV hybrid network with IBR (Fig. 4) and SG (*CASE_1_MV_HYBRID*).

FIGURE 8. SG's (HV network connected) PSCAD model used in *CASE_2A_HV_HYBRID* and *CASE_2B_HV_HYBRID* (Fig. 9).
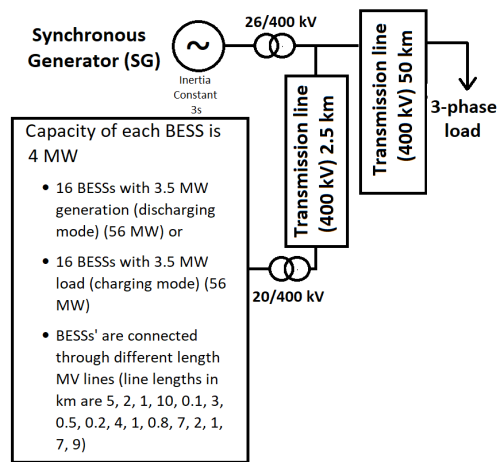

FIGURE 9. One-line diagram of the hybrid small HV network with 16 BESSs (Fig. 6) and SG (Fig. 8) (*CASE_2A_HV_HYBRID*) and (*CASE_2B_HV_HYBRID*).
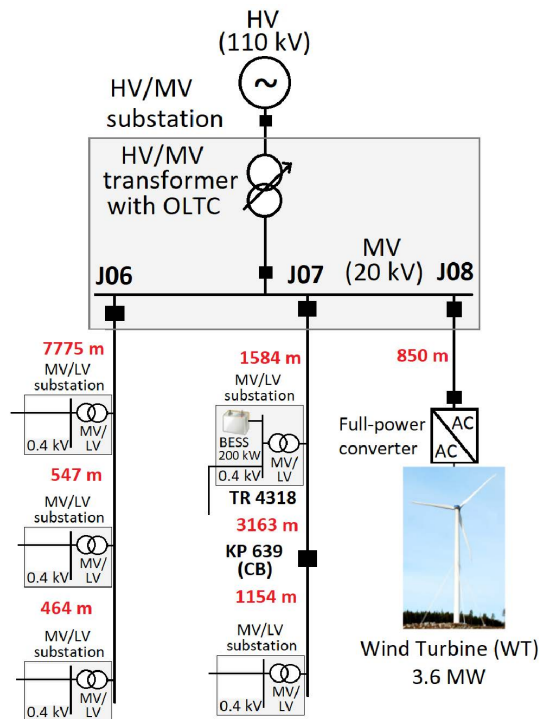

FIGURE 10. One-line diagram of the 100 % IBR-based MV and LV network with WT (MV network, Fig. 4) and BESS (LV network, Fig. 5) in *CASE_1_MV_IBR* and *CASE_1_LV_IBR*.

Lastly, chosen results from hybrid small HV network cases (*CASE_2A_HV_HYBRID* & *CASE_2B_HV_HYBRID*, Fig. 9 and Table 3)) with discharging (Section V.D) and charging (Section V.E) of BESSs are shown.

A. HYBRID MV MICROGRID

The PSCAD simulation results from case *CASE_1_MV _HYBRID* (Fig. 7 and Table 3) subcases (Table 4) are presented in Fig. 12-15. Total simulation time in Table 4 subcases was $t = 30.0$ s and transition to MV islanded (microgrid) operation happened at $t = 13.6$ s.

Fig. 12 shows SG's (Fig. 7) rotating speed behavior after transition to MV islanded (microgrid) operation

in *CASE_1_MV_HYBRID_A (PLL)* and *CASE_1_MV _HYBRID_A (U-FLL)* in which SG operates in GFM control mode with PI-controller (Table 4). It can be seen from Fig. 12, which shows SG rotor speed first swing after islanding, how utilization of GFM U-FLL instead GFL PLL on WT control scheme (Table 4, Fig. 4) supports the transient frequency stability of SG and whole MV microgrid.

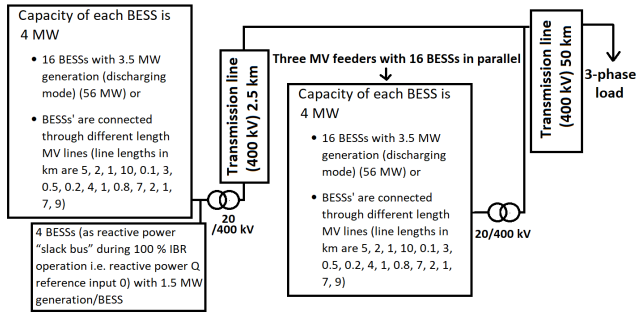In Fig. 13, a comparison of measured frequency and frequency correction set value *w* utilized in U-FLL-based

Capacity of each BESS is 4 MW
- 16 BESSs with 3.5 MW generation (discharging mode) (56 MW) or
- BESSs' are connected through different length MV lines (line lengths in km are 5, 2, 1, 10, 0.1, 3, 0.5, 0.2, 4, 1, 0.8, 7, 2, 1, 7, 9)

Three MV feeders with 16 BESSs in parallel

Capacity of each BESS is 4 MW
- 16 BESSs with 3.5 MW generation (discharging mode) (56 MW) or
- BESSs' are connected through different length MV lines (line lengths in km are 5, 2, 1, 10, 0.1, 3, 0.5, 0.2, 4, 1, 0.8, 7, 2, 1, 7, 9)

4 BESSs (as reactive power "slack bus" during 100 % IBR operation i.e. reactive power Q reference input 0) with 1.5 MW generation/BESS

Transmission line (400 kV) 2.5 km
Transmission line (400 kV) 50 km
20/400 kV
20/400 kV
3-phase load

FIGURE 11. One-line diagram of the 100 % IBR-based small HV network with 68 BESSs (in MV network, Fig. 6) in *CASE_2_HV_IBR*.

TABLE 4. WT and SG control scheme differences in subcases of *CASE_1_MV_HYBRID* (Fig. 7, Table 3).

Subcase	WT control	SG control
CASE_1_MV_HYBRID_A (PLL)	GFL with PLL	GFM (PI-controller)
CASE_1_MV_HYBRID_B (PLL)	GFL with PLL	GFM (P-controller)
CASE_1_MV_HYBRID_C (PLL)	GFL with PLL	GFL with *PQ*-control
CASE_1_MV_HYBRID_A (U-FLL)	GFM with U-FLL (*freq_corr* is adapt., Fig. 1) *)	GFM (PI-controller)
CASE_1_MV_HYBRID_A2 (U-FLL)	GFM with U-FLL (*freq_corr* is 1) *)	GFM (PI-controller)
CASE_1_MV_HYBRID_A3 (U-FLL)	GFM with U-FLL (*freq_corr* is 0.95) *)	GFM (PI-controller)
CASE_1_MV_HYBRID_B (U-FLL)	GFM with U-FLL (*freq_corr* is adapt., Fig. 1) *)	GFM (P-controller)
CASE_1_MV_HYBRID_C1 (U-FLL)	GFM with U-FLL (*freq_corr* is adapt., Fig. 1) **)	GFL with *PQ*-control
CASE_1_MV_HYBRID_C2 (U-FLL)	GFM with U-FLL (*freq_corr* is adapt., Fig. 1) *)	GFL with *PQ*-control

*Q-control input of WT (Fig. 4) is *)non-zero or **) zero during MV islanded (microgrid) operation*
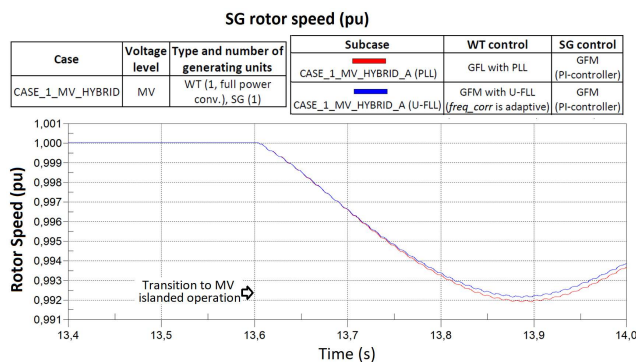
FIGURE 12. SG's rotor speed behavior after transition to MV islanded operation with GFL PLL- or GFM U-FLL-based grid synchronization on WT in *CASE_1_MV_HYBRID_A (PLL)* and *CASE_1_MV_HYBRID_A (U-FLL)* (see Fig. 2, 4, 7 and Table 3 & IV).

synchronization (Fig. 2) of WT (Fig. 4) are shown in *CASE_1_MV_HYBRID_A (U-FLL)* (Table 4). It can be seen that the *w* value corresponds to the proposed grid-forming/-supporting U-FLL main idea presented in Fig. 3 and enables the frequency stability support (Fig. 12) after islanding.
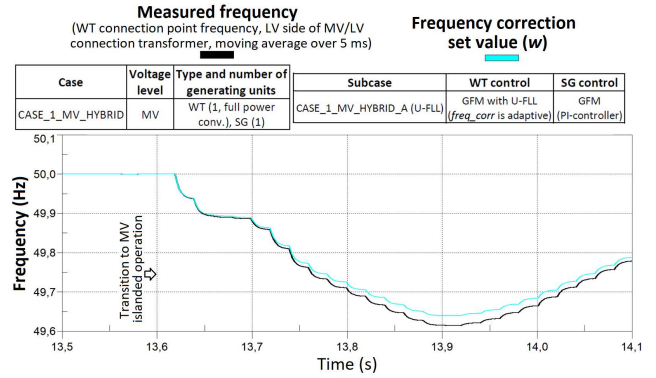
FIGURE 13. Measured frequency and frequency correction set value (*w*) utilized in U-FLL-based synchronization of WT in *CASE_1_MV_HYBRID_A (U-FLL)* (see Fig. 2, 3, 4, 7 and Table 3 & IV).
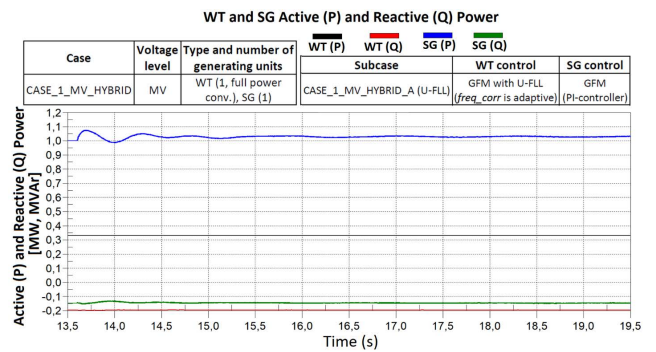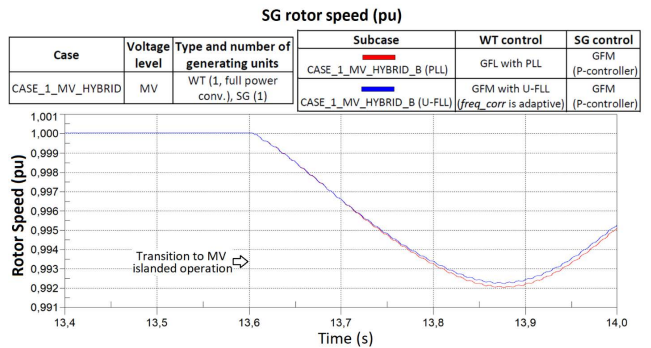
FIGURE 14. Active (*P*) and reactive power (*Q*) behavior of WT and SG in *CASE_1_MV_HYBRID_A (U-FLL)* (see Fig. 2, 3, 4, 7 and Table 3 & IV).

FIGURE 15. SG's rotor speed behavior after transition to MV islanded operation with GFL PLL- or GFM U-FLL-based grid synchronization on WT in *CASE_1_MV_HYBRID_B (PLL)* and *CASE_1_MV_HYBRID_B (U-FLL)* (see Fig. 2, 4, 7 and Table 3 & IV).

In Fig. 14, the active (*P*) and reactive power (*Q*) behavior of WT and SG after transition to MV islanded operation in *CASE_1_MV_HYBRID_A (U-FLL)* (Table 4) are shown. It can be seen that only SG's *P* oscillates notably after the islanding (Fig. 14). In addition, Fig. 14 shows that the utilization of grid-forming U-FLL based synchronization method on WT does not affect its active (*P*) and reactive power (*Q*) output during frequency oscillations after transition to islanded operation.
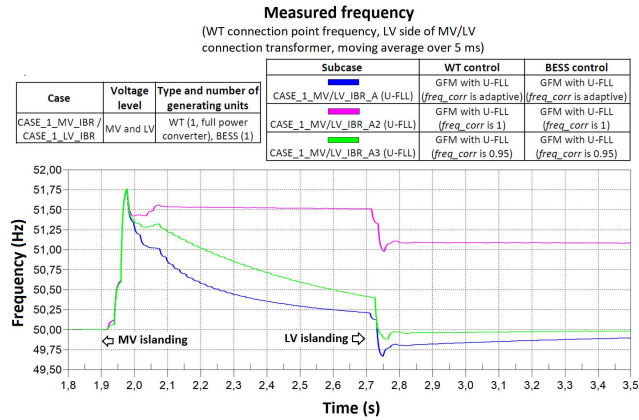
FIGURE 16. Measured frequency at WT connection point with different *freq_corr-* coefficient values (see Fig. 2, 4, 10 and Table 3 & V).
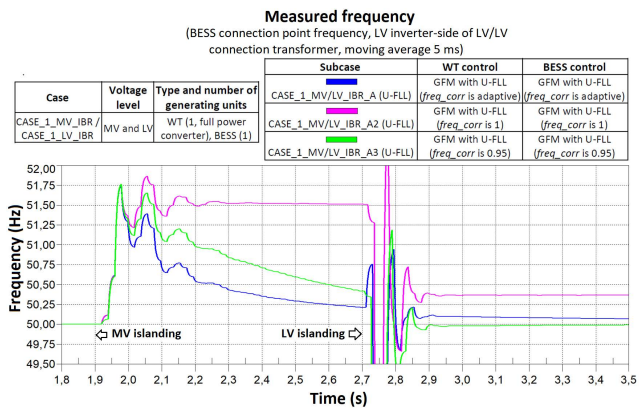

FIGURE 17. Measured frequency at BESS connection point with different *freq_corr-* coefficient values (see Fig. 2, 5, 10 and Table 3 & V).

FIGURE 18. Active (*P*) and reactive power (*Q*) behavior of WT in *CASE_1_MV_IBR_A (U-FLL)* after MV and LV islanding (see Fig. 2, 4, 10 and Table 3 & V).

FIGURE 19. Active (*P*) and reactive power (*Q*) behavior of BESS in *CASE_1_LV_IBR_A (U-FLL)* after MV and LV islanding (see Fig. 2, 5, 10 and Table 3 & V).

TABLE 5. IBR (WT and BESS) control scheme differences in subcases of *CASE_1_MV_IBR* and *CASE_1_LV_IBR* (Fig. 10, Table 3).

Subcase	WT control	BESS control
CASE_1_MV/LV_IBR_A (U-FLL)	GFM with U-FLL (*freq_corr* is adapt., Fig. 1) [*]	GFM with U-FLL (*freq_corr* is adapt., Fig. 1) [**]
CASE_1_MV/LV_IBR_A2 (U-FLL)	GFM with U-FLL (*freq_corr* is 1) [*]	GFM with U-FLL (*freq_corr* is 1) [**]
CASE_1_MV/LV_IBR_A3 (U-FLL)	GFM with U-FLL (*freq_corr* is 0.95) [*]	GFM with U-FLL (*freq_corr* is 0.95) [**]

[*] *Q*-control input of WT (Fig. 4) is zero during MV islanded (microgrid) operation, [*] *Q*-control input of BESS (Fig. 5) is zero during LV islanded (microgrid) operation

Fig. 15 presents the SG's (Fig. 7) rotating speed behavior after islanding in *CASE_1_MV_HYBRID_B (PLL)* and *CASE_1_MV_HYBRID_B (U-FLL)* in which SG operates in GFM control mode with P-controller (Table 4). One can see from Fig. 15 that utilization of GFM U-FLL instead GFL PLL on WT control scheme (Table 4, Fig. 4) supports the transient frequency stability of SG and whole MV microgrid also in this case.

B. 100 % IBR MV AND LV MICROGRID

In the following, the PSCAD simulation results with 100 % IBR-based generation in *CASE_1_MV_IBR* and *CASE_1_LV_IBR* (Fig. 10 and Table 3) subcases (Table 5) are shown in Fig. 16-19. In all subcases (Table 5) WT and BESS are using grid-forming U-FLL-based synchronization. Only frequency correction coefficient (*freq_corr*) value is varied in these subcases (Table 5). Total simulation time in Table 5 subcases was $t = 4.0$ s, transition to MV islanded (microgrid) operation with WT (Fig. 4) and BESS (Fig. 5) happened at $t = 1.9$ s and transition to LV islanded operation with BESS (Fig. 5) happened at $t = 2.7$ s.
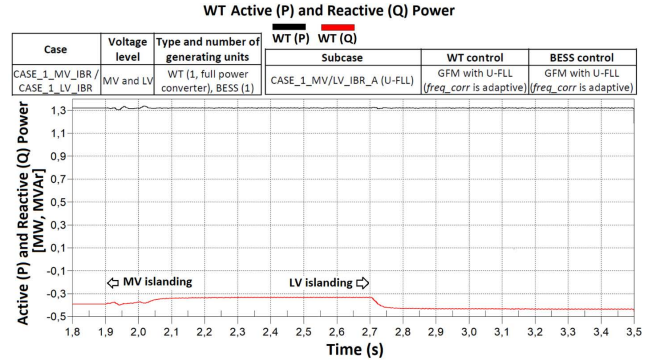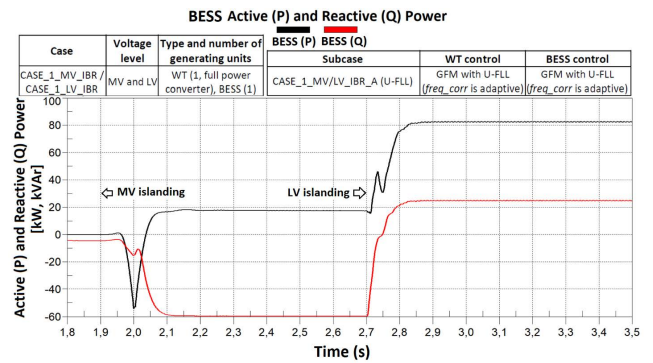
Fig. 16 presents the effect of different *freq_corr* - coefficient values on measured frequency at WT connection point and Fig. 17 at BESS connection point in cases *CASE_1_MV/LV_IBR_A (U-FLL)*, *CASE_1_MV/LV_IBR _A2 (U-FLL)* and *CASE_1_MV/LV_IBR_A3 (U-FLL)* (Table 5). It can be seen from Fig. 16 and 17 that when *freq_corr* value is 1 (*CASE_1_MV/LV_IBR_A2*), steady-state frequency deviation exists after transition to MV islanding as well as after disconnection of LV network section (i.e. LV islanding with BESS). However, with adaptive (frequency-dependent) (Fig. 2) *freq_corr* -coefficient value (*CASE_1_MV/LV_IBR_A*) and *freq_corr* value 0.95

(*CASE_1_MV/LV_IBR_A3*) frequency deviation can be corrected after MV and LV islanding (Fig. 16 and 17). Fig. 17 also shows that after MV islanding the measured frequency at BESS connection point can oscillate a bit more than at WT connection point (Fig. 16).

Fig. 18 and 19 shows the active (*P*) and reactive power (*Q*) behavior of WT (Fig. 18) and BESS (Fig. 19) after MV and LV islanding in *CASE_1_MV_IBR_A (U-FLL)* (Table 5). It can be seen that *P* and *Q* of WT remain quite stable (Fig. 18), but *P* and *Q* of BESS (Fig. 19) change quite notably due to the changes in *P* and *Q* control strategy of BESS (Fig. 5) after topology changes. However, these changes in *P* and *Q* of BESS are not linked to the utilization of grid-forming U-FLL instead of grid-following PLL.

C. SMALL HV NETWORK WITH 100 % IBR-BASED GENERATION

In this section, the PSCAD simulation results with 100 % IBR-based generation (i.e. with 68 BESSs, Fig. 6 and Table 3) in *CASE_2_HV_IBR* (Fig. 11) are presented in Fig. 20-22. More details about *CASE_2_HV_IBR (U-FLL)* are listed below and shown in Fig. 11:

- 68 distributed BESSs (Fig. 6), nominal capacity of each BESS is 4 MW, total generation in the simulation with BESSs is 230 MW
  - 64 BESSs with 3.5 MW generation (224 MW) before changing to *PU*-control at $t = 5.0$ s
  - 4 BESSs (as reactive power ''slack bus'' during 100 % IBR operation i.e. reactive power *Q* reference input 0) with 1.5 MW generation (6 MW active power generation)
- Load at the end of 50 HV transmission line 75 MW in phase A, B and C (total load 225 MW)
- Load increase at the end of 50 km HV transmission line at $t = 15.0$ s (5 MW in phase A, B and C => total load increase 15 MW)
- Total simulation time $t = 25.0$ s.

In Fig. 20, measured frequency at load connection point (Fig. 11) and in Fig. 21 measured frequency and frequency correction set value *w* (Fig. 2) of one BESS (Fig. 6) are shown in *CASE_2_HV_IBR (U-FLL)* with adaptive *freq_corr* value. It can be seen that U-FLL can enable smooth frequency stabilization also in case with 100 % IBR-based small HV network after load increase (Fig. 11, 20 and 21).

Fig. 22a) and in Fig. 22b) show the active (*P_beg*) and reactive power (*Q_beg*) values, respectively, at the beginning of 50 km HV line after load increase in *CASE_2_HV_IBR (U-FLL)*. It can be seen from Fig. 22a) that BESSs *PU*-control increases their active power output after load increase, but it is not linked to the frequency behavior after load increase (Fig. 20). Frequency is kept stable without any steady-state frequency deviation by utilizing the proposed grid-forming U-FLL-based scheme instead of grid-following PLL-based synchronization on BESSs. It can be concluded from simulation results of this Section V.C that the proposed new
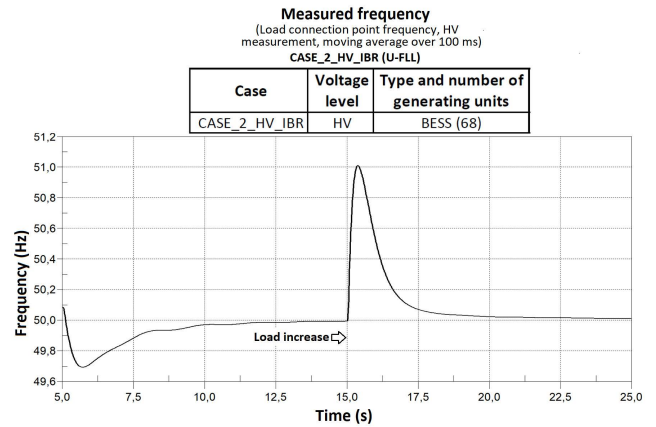

FIGURE 20. Measured frequency at load connection point in *CASE_2_HV_IBR (U-FLL)* (see Fig. 2, 6, 11 and Table 3).
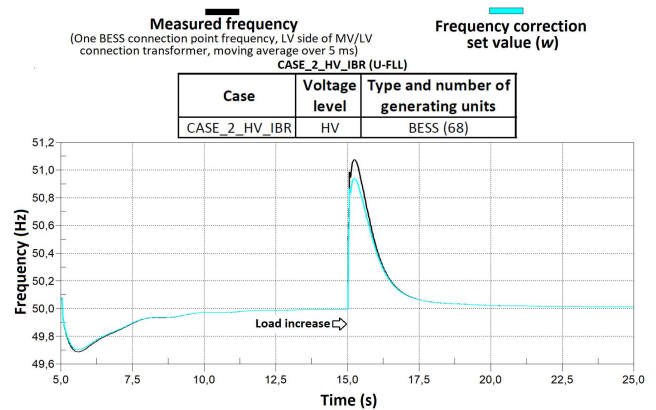

FIGURE 21. Measured frequency and frequency correction set value (*w*) utilized in U-FLL-based synchronization of BESS in *CASE_2_HV_IBR (U-FLL)* (see Fig. 2, 3, 6, 11 and Table 3).

U-FLL-based synchronization can enable stable frequency, also after load increase, in 100 % IBR-based small HV network with 68 BESSs connected in MV network many kilometers away from each other (Fig. 11).

D. HYBRID SMALL HV NETWORK – DISCHARGING OF BESSs

In the following, the PSCAD simulation results from case *CASE_2A_HV_HYBRID* (Fig. 9 and Table 3) with 16 BESSs (Fig. 6) and SG (Fig. 8) are shown in Fig. 23 and 24. More details about compared two subcases *CASE_2A_HV_HYBRID (PLL)* with PLL and *CASE_2A_HV_HYBRID (U-FLL)* with U-FLL are presented below and shown in Fig. 9:

- 16 BESSs (Fig. 6), nominal capacity of each BESS is 4 MW
  - 16 distributed BESSs with 3.5 MW generation (discharging mode) (56 MW)
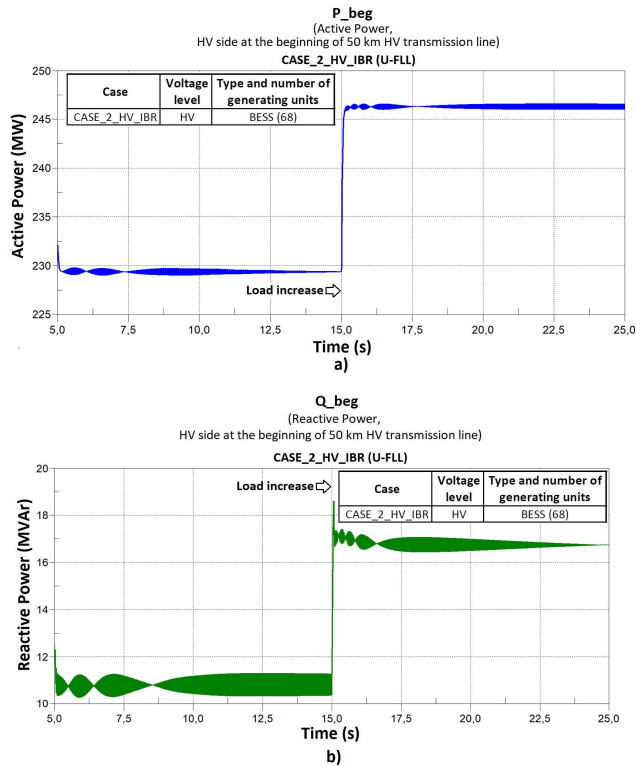- Load at the end of 50 HV transmission line 168.5 MW in phase A, B and C (total load 505.5 MW) (with PLL and U-FLL)

FIGURE 22. a) Active and b) Reactive power values at the beginning of HV line in *CASE_2_HV_IBR (U-FLL)* (see Fig. 2, 6, 11 and Table 3).

- Load increase at the end of 50 km HV transmission line at $t = 5.0$ s (33.33 MW in phase A, B and C => total load increase 100 MW)
- Total simulation time $t = 20.0$ s.

Fig. 23 presents the measured frequencies, calculated from rotating speed of SG (Fig. 8 and 9), after load increase in *CASE_2A_HV_HYBRID (PLL)* and *CASE_2A_HV_HYBRID (U-FLL)*. One can see from Fig. 23 (SG rotor speed first swing after islanding) how utilization of GFM U-FLL instead of GFL PLL on the control scheme of 16 BESSs (Fig. 6) supports the transient first swing frequency stability of SG and HV network.

In Fig. 24 b), the measured frequencies after load increase in *CASE_2A_HV_HYBRID (U-FLL)* and *CASE_2A_HV_HYBRID_2 (U-FLL)* are shown.

In *CASE_2A_HV_HYBRID_2 (U-FLL)* there are 12 discharged BESSs (i.e. 42 MW) more than in *CASE_2A_HV_HYBRID (U-FLL)*, which means that the share of GFM U-FLL and IBR-based generation is also higher when compared to SG-based generation. In addition, in *CASE_2A_HV_HYBRID_2 (U-FLL)* modified adaptive U-FLL coefficient 2 is used (Fig. 24 a) as *freq_corr* -coefficient). One can see from Fig. 24 b) how higher share of GFM U-FLL-based generation supports the frequency stability of SG and HV network. Also the modified adaptive U-FLL coefficient 2 (*freq_corr* -coefficient) had a positive
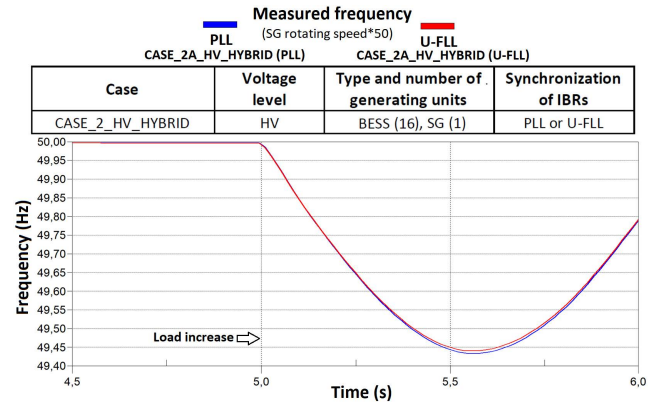

FIGURE 23. Measured frequency calculated from rotor speed of SG after load increase with GFL PLL- or GFM U-FLL-based grid synchronization on discharged BESS in *CASE_2A_HV_HYBRID (PLL)* and *CASE_2A_HV_HYBRID (U-FLL)* (see Fig. 2, 6, 8, 9 and Table 3).
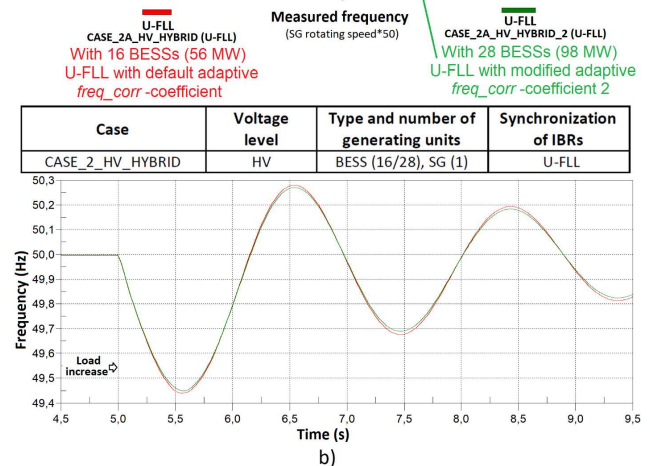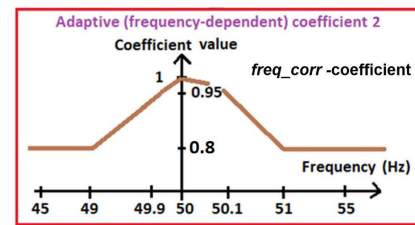

FIGURE 24. a) Modified adaptive U-FLL coefficient 2 (*freq_corr* -coefficient) and b) measured frequency calculated from rotor speed of SG after load increase with GFM U-FLL-based grid synchronization on discharged BESS in CASE_2A_HV_HYBRID (U-FLL) and CASE_2A_HV_HYBRID_2 (U-FLL) (see Fig. 2, 6, 8, 9 and Table 3).

impact, but it was minor when compared to increased share of GFM U-FLL-based generation.

E. HYBRID SMALL HV NETWORK – CHARGING OF BESSs
In this section, the PSCAD simulation results from case *CASE_2B_HV_HYBRID* (Fig. 9 and Table 3) with 16 charged BESSs (Fig. 6) acting as loads and SG (Fig. 7) are shown in Fig. 25 and 26. More details about compared three subcases *CASE_2A_HV_HYBRID (SG only)*, *CASE_2B_HV_HYBRID*
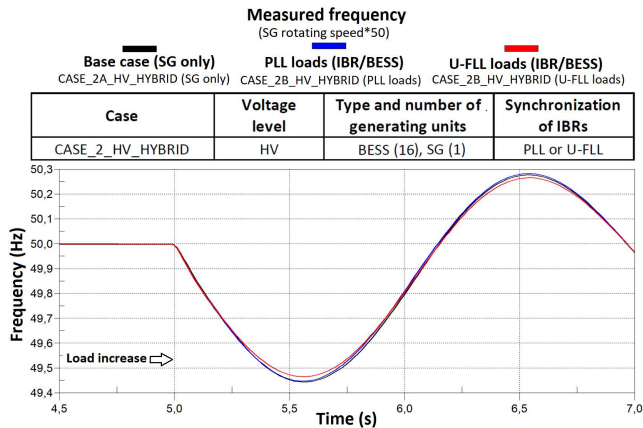
FIGURE 25. Measured frequency calculated from rotor speed of SG after load increase with GFL PLL- or GFM U-FLL-based grid synchronization on charged BESS in *CASE_2A_HV_HYBRID (SG only)*, *CASE_2B_HV_HYBRID (PLL loads)* and *CASE_2B_HV_HYBRID (U-FLL loads)* (see Fig. 2, 6, 8, 9 and Table 3).

FIGURE 26. Measured frequency calculated from rotor speed of SG after load increase with GFM U-FLL-based grid synchronization on charged BESS in *CASE_2B_HV_HYBRID (U-FLL loads)* and *CASE_2B_HV_HYBRID_2 (U-FLL loads)* (see Fig. 2, 6, 8, 9 and Table 3).

(PLL) with PLL and *CASE_2B_HV_HYBRID (U-FLL)* with U-FLL are presented below and shown in Fig. 9:

- 16 distributed BESSs (Fig. 6), nominal capacity of each BESS is 4 MW
  - 16 BESSs with 3.5 MW load (charging mode) (56 MW)
- Load at the end of 50 HV transmission line 150 MW in phase A, B and C (total load 450 MW) (base case with SG only i.e. no IBR-based generation or loads)
- Load at the end of 50 HV transmission line 131.5 MW in phase A, B and C (total load 394.5 MW + 56 MW (BESSs charging) = 450.5 MW) (with PLL loads and U-FLL loads)
- Load increase at the end of 50 km HV transmission line at $t = 5.0$ s (33.33 MW in phase A, B and C => total load increase 100 MW)
- Total simulation time $t = 20.0$ s.

In Fig. 25, the measured frequencies, calculated from rotating speed of SG (Fig. 8 and 9), after load increase in *CASE_2A_HV_HYBRID (SG only)*, *CASE_2B_HV_HYBRID (PLL loads)* and *CASE_2B_HV_HYBRID (U-FLL loads)* are shown. It can be seen from Fig. 25 (SG rotor speed first swing after islanding) that utilization of GFM U-FLL instead GFL PLL on the control scheme of 16 BESSs (Fig. 6) supports the transient frequency stability of SG and HV network also when BESSs are charged as IBR-based loads.

Fig. 26 presents the measured frequencies after load increase in *CASE_2B_HV_HYBRID (U-FLL loads)* and *CASE_2B_HV_HYBRID_2 (U-FLL loads)*. In *CASE_2B_HV_HYBRID_2 (U-FLL loads)* there are 12 charged BESSs (i.e. 42 MW) more than in *CASE_2B_HV_HYBRID (U-FLL loads)*, which means that the share of GFM U-FLL and IBR-based load is higher when compared to passive load. It can be seen from Fig. 26 that higher share of GFM U-FLL-based load supports the frequency stability of SG especially during the first swings. On the other hand, it can be mentioned
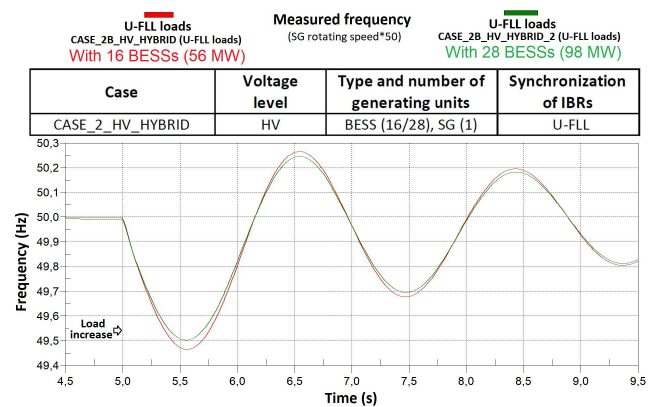
that the modification of adaptive *freq_corr* -coefficient (like in Fig. 24) with U-FLL based loads may have a different impact on frequency stability than with U-FLL based generating units. However, adaptive *freq_corr* -coefficient (shown in Fig. 2) was found to have positive impact on frequency stability in all studied cases. Therefore, it has been used as a default *freq_corr* -coefficient value in the simulation studies of this paper.

VI. CONCLUSION

No universal grid-forming control and synchronization method currently exists and therefore, this paper tried to propose new universal grid-forming/-supporting U-FLL-based synchronization for IBRs. This paper focused only on presenting the new grid-forming and supporting U-FLL synchronization method without focusing on simultaneous active power control utilization for frequency stability improvement (e.g. by *Pf*-control of BESS) which will be focused on in future studies. In addition, the proposed new grid-forming U-FLL method has also other advantageous features over some previously proposed GFM control methods during operation in 100 % IBR-based systems (e.g. microgrids) like, for example, zero steady-state frequency deviation and compatibility with existing passive islanding detection schemes.

To comprehensively study the operation and confirm the applicability of the proposed new U-FLL method, multiple PSCAD simulation studies were done with different shares of IBR-based generation. Based on the simulation results following conclusions were made:

- Simulation results with both hybrid power systems, a) MV network hybrid microgrid and b) hybrid small HV network, showed that utilization of GFM U-FLL instead of GFL PLL on IBR-based WT and BESS supported the transient SG first swing frequency stability after MV islanding and load increase in HV network. In addition, the simulations confirmed the positive effect of adaptive *freq_corr* -coefficient on frequency stability after transition to MV islanded operation.

- Larger share of U-FLL-based generation or load in hybrid HV network improved the frequency stability especially during the first swings after load increase.
- From simulation results it was confirmed that the proposed U-FLL with adaptive *freq_corr* value enables also smooth frequency stabilization after MV and LV islanding in 100 % IBR-based MV and LV microgrids.
- Simulation results showed that the new U-FLL-based synchronization can enable stable power system frequency after load increase also in 100 % IBR-based small HV network with 68 distributed BESSs connected in MV network many kilometers away from each other.
- In addition, simulation results proved that utilization of grid-supporting U-FLL instead GFL PLL on 16 distributed IBR-based loads can also support the transient first swing frequency stability of SG and HV network.

In overall, it can be concluded based on the simulation results, that general targets 1)-4) for the new U-FLL described in Section III.A were achieved. These targets included 1) applicability of U-FLL on different type of variable inertia, hybrid power systems and utilization capability for intended islanded operation, 2) possibility to retrofit the existing PLL-based GFL control schemes with grid-forming features of U-FLL, 3) consider the possibility of making or retrofitting PLL-based grid-following inverter-interfaced loads with U-FLL to be more grid-supporting and 4) zero steady-state frequency deviation during 100 % IBR-based operation (e.g. islanded microgrid operation) from nominal frequency. Fulfillment of targets 5) and 6) (Section III.A) will be done in further studies with more in-depth stability analysis. In addition, the functionality of the proposed U-FLL needs to be also verified with laboratory testing before real-life experiments.

REFERENCES

[1] B. Mohandes, M. S. E. Moursi, N. Hatziargyriou, and S. E. Khatib, "A review of power system flexibility with high penetration of renewables," *IEEE Trans. Power Syst.*, vol. 34, no. 4, pp. 3140–3155, Jul. 2019.

[2] H. Laaksonen, H. Khajeh, C. Parthasarathy, M. Shafie-Khah, and N. Hatziargyriou, "Towards flexible distribution systems: Future adaptive management schemes," *Appl. Sci.*, vol. 11, no. 8, p. 3709, Apr. 2021, doi: 10.3390/app11083709.

[3] R. Brazier, L. Cunha, P. Hermans, G. de Jong, T. Knop, M. Lallemand, M. Merkel, A. S. Risnes, M. de la Torre Rodríguez, and P. de Wit, "TSO—DSO report, an integrated approach to active system management with the focus on TSO—DSO coordination in congestion management and balancing," ENTSO-E, EDSO, EURELECTRIC, CEDEC, GEODE, Brussels, Belgium, Tech. Rep., 2019. [Online]. Available: https://eepublicdownloads.entsoe.eu/clean-documents/Publications/Position%20papers%20and%20reports/TSO-DSO_ASM_2019_190416.pdf and https://docstore.entsoe.eu/Documents/Publications/Position%20papers%20and%20reports/TSO-DSO_ASM_2019_190416.pdf

[4] H. Laaksonen, C. Parthasarathy, H. Khajeh, M. Shafie-Khah, and N. Hatziargyriou, "Flexibility services provision by frequency-dependent control of on-load tap-changer and distributed energy resources," *IEEE Access*, vol. 9, pp. 45587–45599, 2021, doi: 10.1109/ACCESS.2021.3067297.

[5] M. G. Dozein, A. M. De Corato, and P. Mancarella, "Virtual inertia response and frequency control ancillary services from hydrogen electrolyzers," *IEEE Trans. Power Syst.*, early access, Jun. 10, 2022, doi: 10.1109/TPWRS.2022.3181853.

[6] X. Wang, M. G. Taul, H. Wu, Y. Liao, F. Blaabjerg, and L. Harnefors, "Grid-synchronization stability of converter-based resources—An overview," *IEEE Open J. Ind. Appl.*, vol. 1, pp. 115–134, 2020, doi: 10.1109/OJIA.2020.3020392.

[7] F. Milano, F. Dorfler, G. Hug, D. J. Hill, and G. Verbic, "Foundations and challenges of low-inertia systems," in *Proc. Power Syst. Comput. Conf. (PSCC)*, Jun. 2018, pp. 1–25, doi: 10.23919/PSCC.2018.8450880.

[8] R. H. Lasseter, Z. Chen, and D. Pattabiraman, "Grid-forming inverters: A critical asset for the power grid," *IEEE J. Emerg. Sel. Topics Power Electron.*, vol. 8, no. 2, pp. 925–935, Jun. 2020, doi: 10.1109/JESTPE.2019.2959271.

[9] L. Yashen, "Final technical report: Stabilizing the power system in 2035 and beyond-evolving from grid-following to grid-forming distributed inverter controllers," Nat. Renew. Energy Lab., Golden, CO, USA, Tech. Rep., NREL/TP-5D00-79761, 2021. [Online]. Available: https://www.nrel.gov/docs/fy21osti/79761.pdf

[10] L. Yashen, J. H. Eto, B. B. Johnson, J. D. Flicker, R. H. Lasseter, H. N. V. Pico, G.-S. Seo, B. J. Pierre, and A. Ellis, "Research roadmap on grid-forming inverters," Nat. Renew. Energy Lab., Golden, CO, USA, Tech. Rep., NREL/TP-5D00-73476, 2020. [Online]. Available: https://www.nrel.gov/docs/fy21osti/73476.pdf

[11] R. Rosso, X. Wang, M. Liserre, X. Lu, and S. Engelken, "Grid-forming converters: Control approaches, grid-synchronization, and future trends—A review," *IEEE Open J. Ind. Appl.*, vol. 2, pp. 93–109, 2021, doi: 10.1109/OJIA.2021.3074028.

[12] J. Rocabert, A. Luna, F. Blaabjerg, and P. Rodríguez, "Control of power converters in AC microgrids," *IEEE Trans. Power Electron.*, vol. 27, no. 11, pp. 4734–4749, Dec. 2012.

[13] M. Paolone, T. Gaunt, X. Guillaud, M. Liserre, S. Meliopoulos, A. Monti, T. Van Cutsem, V. Vittal, and C. Vournas, "Fundamentals of power systems modelling in the presence of converter-interfaced generation," *Electr. Power Syst. Res.*, vol. 189, Dec. 2020, Art. no. 106811.

[14] J. Matevosyan, B. Badrzadeh, T. Prevost, E. Quitmann, D. Ramasubramanian, H. Urdal, and S. Achilles, "Grid-forming inverters: Are they the key for high renewable penetration?" *IEEE Power Energy Mag.*, vol. 17, no. 6, pp. 89–98, Nov. 2019.

[15] (2022). *OSMOSE—Final Report*. [Online]. Available: https://www.osmose-h2020.eu/wp-content/uploads/2022/03/OSMOSE-Final-Brochure-Full-version.pdf

[16] R. Teodorescu, M. Liserre, and P. Rodriguez, *Grid Converters for Photovoltaic and Wind Power Systems*. Hoboken, NJ, USA: Wiley, 2011.

[17] A. Luna, J. Rocabert, J. I. Candela, J. R. Hermoso, R. Teodorescu, F. Blaabjerg, and P. Rodrigue, "Grid voltage synchronization for distributed generation systems under grid fault conditions," *IEEE Trans. Ind. Appl.*, vol. 51, no. 4, pp. 3414–3425, Aug. 2015.

[18] X. Wang and F. Blaabjerg, "Harmonic stability in power electronic-based power systems: Concept, modeling, and analysis," *IEEE Trans. Smart Grid*, vol. 10, no. 3, pp. 2858–2870, May 2019.

[19] M. G. Taul, X. Wang, P. Davari, and F. Blaabjerg, "An overview of assessment methods for synchronization stability of grid-connected converters under severe symmetrical grid faults," *IEEE Trans. Power Electron.*, vol. 34, no. 10, pp. 9655–9670, Oct. 2019.

[20] L. Zhang, L. Harnefors, and H.-P. Nee, "Power-synchronization control of grid-connected voltage-source converters," *IEEE Trans. Power Syst.*, vol. 25, no. 2, pp. 809–820, May 2010.

[21] P. Unruh, M. Nuschke, P. Strauß, and F. Welck, "Overview on grid-forming inverter control methods," *Energies*, vol. 13, no. 10, p. 2589, May 2020, doi: 10.3390/EN13102589.

[22] E. Rokrok, T. Qoria, A. Bruyere, B. Francois, and X. Guillaud, "Effect of using PLL-based grid-forming control on active power dynamics under various SCR," in *Proc. 45th Annu. Conf. IEEE Ind. Electron. Soc.*, Lisbon, Portugal, Oct. 2019, pp. 4799–4804.

[23] L. Harnefors, M. Schweizer, J. Kukkola, M. Routimo, M. Hinkkanen, and X. Wang, "Generic PLL-based grid-forming control," *IEEE Trans. Power Electron.*, vol. 37, no. 2, pp. 1201–1204, Feb. 2022, doi: 10.1109/TPEL.2021.3106045.

[24] S. Dong and Y. C. Chen, "Adjusting synchronverter dynamic response speed via damping correction loop," *IEEE Tran Energy Convers.*, vol. 32, no. 2, pp. 608–619, Jun. 2017.

[25] D. Chen, Y. Xu, and A. Q. Huang, "Integration of DC microgrids as virtual synchronous machines into the AC grid," *IEEE Trans. Ind. Electron.*, vol. 64, no. 9, pp. 7455–7466, Sep. 2017.

[26] A. Crivellaro, A. Tayyebi, C. Gavriluta, D. Groß, A. Anta, F. Kupzog, and F. Dörfler, "Beyond low-inertia systems: Massive integration of grid-forming power converters in transmission grids," in *Proc. IEEE Power Energy Soc. Gen. Meeting (PESGM)*, Aug. 2020, pp. 1–5, doi: 10.1109/PESGM41954.2020.9282031.

[27] M. O'Malley, T. Bowen, J. Bialek, M. Braun, N. Cutululis, T. Green, A. Hansen, E. Kennedy, J. Kiviluoma, J. Leslie, Y. Li, J. Matevosyan, J. McDowell, N. Miller, P. Pettingill, D. Ramasubramanian, L. Robinson, C. Schaefer, and J. Ward, "Enabling power system transformation globally: A system operator research agenda for bulk power system issues," *IEEE Power Energy Mag.*, vol. 19, no. 6, pp. 45–55, Nov. 2021, doi: 10.1109/MPE.2021.3104078.

[28] B. Wen, D. Boroyevich, R. Burgos, P. Mattavelli, and Z. Shen, "Analysis of D-Q small-signal impedance of grid-tied inverters," *IEEE Trans. Power Electron.*, vol. 31, no. 1, pp. 675–687, Jan. 2016.

[29] J. Z. Zhou, H. Ding, S. Fan, Y. Zhang, and A. M. Gole, "Impact of short-circuit ratio and phase-locked-loop parameters on the small-signal behavior of a VSC-HVDC converter," *IEEE Trans. Power Del.*, vol. 29, no. 5, pp. 2287–2296, Oct. 2014.

[30] R. Rosso, M. Andresen, S. Engelken, and M. Liserre, "Analysis of the interaction among power converters through their synchronization mechanism," *IEEE Trans. Power Electron.*, vol. 34, no. 12, pp. 12321–12332, Dec. 2019, doi: 10.1109/TPEL.2019.2905355.

[31] R. Rosso, J. Cassoli, G. Buticchi, S. Engelken, and M. Liserre, "Robust stability analysis of LCL filter based synchronverter under different grid conditions," *IEEE Trans. Power Electron.*, vol. 34, no. 6, pp. 5842–5853, Jun. 2018.

[32] R. Rosso, S. Engelken, and M. Liserre, "Robust stability analysis of synchronverters operating in parallel," *IEEE Trans. Power Electron.*, vol. 34, no. 1, pp. 11309–11319, Nov. 2019.

[33] Y. Liao, X. Wang, F. Liu, K. Xin, and Y. Liu, "Sub-synchronous control interaction in grid-forming VSCs with droop control," in *Proc. 4th IEEE Workshop Electron. Grid (eGRID)*, Nov. 2019, pp. 1–6.

[34] M. G. Taul, S. Golestan, X. Wang, P. Davari, and F. Blaabjerg, "Modeling of converter synchronization stability under grid faults: The general case," *IEEE J. Emerg. Sel. Topics Power Electron.*, vol. 10, no. 3, pp. 2790–2804, Jun. 2022, doi: 10.1109/JESTPE.2020.3024940.

[35] G. Li, Y. Chen, A. Luo, Z. He, H. Wang, Z. Zhu, W. Wu, and L. Zhou, "Analysis and mitigation of subsynchronous resonance in series-compensated grid-connected system controlled by a virtual synchronous generator," *IEEE Trans. Power Electron.*, vol. 35, no. 10, pp. 11096–11107, Oct. 2020.

[36] T. Liu, X. Wang, F. Liu, K. Xin, and Y. Liu, "Islanding detection of grid-forming inverters: Mechanism, methods, and challenges," *IEEE Electrific. Mag.*, vol. 10, no. 1, pp. 30–38, Mar. 2022, doi: 10.1109/MELE.2021.3139206.

[37] Q.-C. Zhong and G. Weiss, "Synchronverters: Inverters that mimic synchronous generators," *IEEE Trans. Ind. Electron.*, vol. 58, no. 4, pp. 1259–1267, Apr. 2011.

[38] S. D'Arco, J. A. Suul, and O. B. Fosso, "A virtual synchronous machine implementation for distributed control of power converters in smartgrids," *Electr. Power Syst. Res.*, vol. 122, pp. 180–197, May 2015.

[39] J. Liu, Y. Miura, and T. Ise, "Comparison of dynamic characteristics between virtual synchronous generator and droop control in inverter-based distributed generators," *IEEE Trans. Power Electron.*, vol. 31, no. 5, pp. 3600–3611, May 2016.

[40] T. Dragicevic, S. Vazquez, and P. Wheeler, "Advanced control methods for power converters in DG systems and microgrids," *IEEE Trans. Ind. Electron.*, vol. 68, no. 7, pp. 5847–5862, Jul. 2021, doi: 10.1109/TIE.2020.2994857.

[41] S. Golestan, J. M. Guerrero, and J. C. Vasquez, "Three-phase PLLs: A review of recent advances," *IEEE Trans. Power Electron.*, vol. 32, no. 3, pp. 1894–1907, Mar. 2017.

[42] W. Zhang, J. Rocabert, J. I. Candela, and P. Rodriguez, "Synchronous power control of grid-connected power converters under asymmetrical grid fault," *Energies*, vol. 10, no. 7, pp. 1–21, 2017.

[43] Q.-C. Zhong, P.-L. Nguyen, Z. Ma, and W. Sheng, "Self-synchronized synchronverters: Inverters without a dedicated synchronization unit," *IEEE Trans. Power Electron.*, vol. 29, no. 2, pp. 617–630, Feb. 2014.

[44] H. Wu and X. Wang, "Design-oriented transient stability analysis of PLL-synchronized voltage-source converters," *IEEE Trans. Power Electron.*, vol. 35, no. 4, pp. 3573–3589, Apr. 2020.

[45] H. Wu and X. Wang, "Design-oriented transient stability analysis of grid-connected converters with power synchronization control," *IEEE Trans. Ind. Electron.*, vol. 66, no. 8, pp. 6473–6482, Aug. 2019.

[46] D. Pan, X. Wang, F. Liu, and R. Shi, "Transient stability of voltage-source converters with grid-forming control: A design-oriented study," *IEEE J. Emerg. Sel. Topics Power Electron.*, vol. 8, no. 2, pp. 1019–1033, Jun. 2020.

[47] T. Qoria, F. Gruson, F. Colas, G. Denis, T. Prevost, and X. Guillaud, "Critical clearing time determination and enhancement of grid-forming converters embedding virtual impedance as current limitation algorithm," *IEEE J. Emerg. Sel. Topics Power Electron.*, vol. 8, no. 2, pp. 1050–1061, Jun. 2020.

[48] N. Hatziargyriou, J. Milanovic, C. Rahmann, V. Ajjarapu, C. Canizares, I. Erlich, D. Hill, I. Hiskens, I. Kamwa, B. Pal, P. Pourbeik, J. Sanchez-Gasca, A. Stankovic, T. Van Cutsem, V. Vittal, and C. Vournas, "Definition and classification of power system stability—Revisited & extended," *IEEE Trans. Power Syst.*, vol. 36, no. 4, pp. 3271–3281, Jul. 2021, doi: 10.1109/TPWRS.2020.3041774.

[49] J. Matevosyan, J. MacDowell, N. Miller, B. Badrzadeh, D. Ramasubramanian, A. Isaacs, R. Quint, E. Quitmann, R. Pfeiffer, H. Urdal, T. Prevost, V. Vittal, D. Woodford, S. H. Huang, and J. O'Sullivan, "A future with inverter-based resources: Finding strength from traditional weakness," *IEEE Power Energy Mag.*, vol. 19, no. 6, pp. 18–28, Nov. 2021, doi: 10.1109/MPE.2021.3104075.

[50] E. Ebrahimzadeh, F. Blaabjerg, X. Wang, and C. L. Bak, "Harmonic stability and resonance analysis in large PMSG-based wind power plants," *IEEE Trans. Sustain. Energy*, vol. 9, no. 1, pp. 12–23, Jan. 2018.

[51] M. Li, Y. Wang, W. Hu, S. Shu, P. Yu, Z. Zhang, and F. Blaabjerg, "Unified modeling and analysis of dynamic power coupling for grid-forming converters," *IEEE Trans. Power Electron.*, vol. 37, no. 2, pp. 2321–2337, Feb. 2022, doi: 10.1109/TPEL.2021.3107329.

[52] U. Markovic, J. Vorwerk, P. Aristidou, and G. Hug, "Stability analysis of converter control modes in low-inertia power systems," in *Proc. IEEE PES Innov. Smart Grid Technol. Conf. Eur. (ISGT-Europe)*, Oct. 2018, pp. 1–6, doi: 10.1109/ISGTEurope.2018.8571583.

[53] L. Ding, X. Lu, and J. Tan, "Comparative small-signal stability analysis of grid-forming and grid-following inverters in low-inertia power systems," in *Proc. 47th Annu. Conf. IEEE Ind. Electron. Soc.*, Oct. 2021, pp. 1–6, doi: 10.1109/IECON48115.2021.9589651.

[54] L. Ding, Y. Men, Y. Du, X. Lu, B. Chen, J. Tan, and Y. Lin, "Region-based stability analysis of resilient distribution systems with hybrid grid-forming and grid-following inverters," in *Proc. IEEE Energy Convers. Congr. Expo. (ECCE)*, Oct. 2020, pp. 3733–3740, doi: 10.1109/ECCE44975.2020.9236196.

[55] Z. Dai, G. Li, M. Fan, J. Huang, Y. Yang, and W. Hang, "Global stability analysis for synchronous reference frame phase-locked loops," *IEEE Trans. Ind. Electron.*, vol. 69, no. 10, pp. 10182–10191, Oct. 2022, doi: 10.1109/TIE.2021.3125655.

[56] S. Khan, B. Bletterie, A. Anta, and W. Gawlik, "On small signal frequency stability under virtual inertia and the role of PLLs," *Energies*, vol. 11, no. 9, p. 2372, Sep. 2018, doi: 10.3390/en11092372.

[57] M. Ghazavi Dozein, B. C. Pal, and P. Mancarella, "Dynamics of inverter-based resources in weak distribution grids," *IEEE Trans. Power Syst.*, vol. 37, no. 5, pp. 3682–3692, Sep. 2022, doi: 10.1109/TPWRS.2022.3142016.

[58] A. Tayyebi, D. Groß, A. Anta, F. Kupzog, and F. Dörfler, "Frequency stability of synchronous machines and grid-forming power converters," *IEEE J. Emerg. Sel. Topics Power Electron.*, vol. 8, no. 2, pp. 1004–1018, Jun. 2020, doi: 10.1109/JESTPE.2020.2966524.

[59] A. Tuckey and S. Round, "Grid-forming inverters for grid-connected microgrids: Developing 'good citizens' to ensure the continued flow of stable, reliable power," *IEEE Electrific. Mag.*, vol. 10, no. 1, pp. 39–51, Mar. 2022, doi: 10.1109/MELE.2021.3139172.

[60] M. Chen, D. Zhou, A. Tayyebi, E. Prieto-Araujo, F. Dorfler, and F. Blaabjerg, "Generalized multivariable grid-forming control design for power converters," *IEEE Trans. Smart Grid*, vol. 13, no. 4, pp. 2873–2885, Jul. 2022, doi: 10.1109/TSG.2022.3161608.

[61] D. Yang, X. Wang, F. Blaabjerg, F. Liu, K. Xin, and Y. Liu, "Complex-vector PLL for enhanced synchronization with weak power grids," in *Proc. IEEE 19th Workshop Control Modeling Power Electron. (COMPEL)*, Jun. 2018, pp. 1–6, doi: 10.1109/COMPEL.2018.8459976.

[62] S. Zhou, X. Zou, D. Zhu, Li Tong, Y. Zhao, Y. Kang, and X. Yuan, "An improved design of current controller for LCL-type grid-connected converter to reduce negative effect of PLL in weak grid," *IEEE J. Emerg. Sel. Topics Power Electron.*, vol. 6, no. 2, pp. 648–663, Dec. 2018, doi: 10.1109/JESTPE.2017.2780918.

[63] A. Adib and B. Mirafzal, "Virtual inductance for stable operation of grid-interactive voltage source inverters," *IEEE Trans. Ind. Electron.*, vol. 66, no. 8, pp. 6002–6011, Aug. 2019, doi: 10.1109/TIE.2018.2874594.

[64] Y. Gui, X. Wang, H. Wu, and F. Blaabjerg, "Voltage-modulated direct power control for a weak grid-connected voltage source inverters," *IEEE Trans. Power Electron.*, vol. 34, no. 11, pp. 11383–11395, Nov. 2019, doi: 10.1109/TPEL.2019.2898268.

[65] L. Huang, C. Wu, D. Zhou, and F. Blaabjerg, "A double-PLLs-based impedance reshaping method for extending stability range of grid-following inverter under weak grid," *IEEE Trans. Power Electron.*, vol. 37, no. 4, pp. 4091–4104, Apr. 2022, doi: 10.1109/TPEL.2021.3127644.

[66] L. Harnefors, J. Kukkola, M. Routimo, M. Hinkkanen, and X. Wang, "A universal controller for grid-connected voltage-source converters," *IEEE J. Emerg. Sel. Topics Power Electron.*, vol. 9, no. 5, pp. 5761–5770, Oct. 2021, doi: 10.1109/JESTPE.2020.3039407.

[67] P. Rodriguez, A. Luna, M. Ciobotaru, R. Teodorescu, and F. Blaabjerg, "Advanced grid synchronization system for power converters under unbalanced and distorted operating conditions," in *Proc. 32nd Annu. Conf. IEEE Ind. Electron.*, Nov. 2006, pp. 5173–5178, doi: 10.1109/IECON.2006.347807.

[68] P. Rodriguez, A. Luna, I. Candela, R. Mujal, R. Teodorescu, and F. Blaabjerg, "Multiresonant frequency-locked loop for grid synchronization of power converters under distorted grid conditions," *IEEE Trans. Ind. Electron.*, vol. 58, no. 1, pp. 127–138, Jan. 2011, doi: 10.1109/TIE.2010.2042420.

[69] H. Ahmed, S.-A. Amamra, and M. Bierhoff, "Frequency-locked loop-based estimation of single-phase grid voltage parameters," *IEEE Trans. Ind. Electron.*, vol. 66, no. 11, pp. 8856–8859, Nov. 2019, doi: 10.1109/TIE.2018.2873527.

[70] A. Bamigbade, V. Khadkikar, H. Zeineldin, M. S. ElMoursi, and M. A. Hosani, "Single-phase transfer delay FLL with enhanced performance for power system applications," *IEEE J. Emerg. Sel. Topics Power Electron.*, vol. 10, no. 1, pp. 349–360, Feb. 2022, doi: 10.1109/JESTPE.2021.3069504.

[71] M. Saeedian, S. Taheri, and E. Pouresmaeil, "Double–stage photovoltaic generator augmented with FLL–based synthetic inertia emulator," *Electr. Power Syst. Res.*, vol. 204, Mar. 2022, Art. no. 107715.

[72] Q.-C. Zhong, W.-L. Ming, and Y. Zeng, "Self-synchronized universal droop controller," *IEEE Access*, vol. 4, pp. 7145–7153, 2016, doi: 10.1109/ACCESS.2016.2616115.

[73] Q.-C. Zhong, "Power-electronics-enabled autonomous power systems: Architecture and technical routes," *IEEE Trans. Ind. Electron.*, vol. 64, no. 7, pp. 5907–5918, Jul. 2017, doi: 10.1109/TIE.2017.2677339.

[74] F. Blaabjerg, R. Teodorescu, M. Liserre, and A. V. Timbus, "Overview of control and grid synchronization for distributed power generation systems," *IEEE Trans. Ind. Electron.*, vol. 53, no. 5, pp. 1398–1409, Oct. 2006, doi: 10.1109/TIE.2006.881997.

[75] W. Sang, W. Guo, S. Dai, C. Tian, S. Yu, and Y. Teng, "Virtual synchronous generator, a comprehensive overview," *Energies*, vol. 15, no. 17, p. 6148, Aug. 2022, doi: 10.3390/en15176148.

HANNU LAAKSONEN (Member, IEEE) received the M.Sc. (Tech.) degree in electrical power engineering from the Tampere University of Technology, Tampere, Finland, in 2004, and the Ph.D. (Tech.) degree in electrical engineering from the University of Vaasa, Vaasa, Finland, in 2011. His employment experience includes working as a Research Scientist at the VTT Technical Research Centre of Finland and the University of Vaasa. He has worked as a Principal Engineer at ABB Ltd., Vaasa. He is currently a Professor in electrical engineering at the University of Vaasa. He is also Flexible Energy Resources—the Research Team Leader and the Manager of the Smart Energy Master's Program. His research interests include the control and protection of low-inertia power systems and microgrids, active management of distributed and flexible energy resources in future smart energy systems, and future-proof technology and market concepts for smart grids.

○ ○ ○